peroxidase activity was blocked with 0.3% H_2O_2 in methanol. The sections were exposed to 1% BSA in PBS and were then incubated overnight at 4°C with goat anti-CD3ε (M-20; Santa Cruz Biotechnology Inc.). Immune complexes were labeled with biotinylated anti-goat IgG and streptavidin alkaline phosphatase (Nichirei). The signals were visualized with a Vector Blue Alkaline Phosphatase Substrate Kit (Vector Laboratories). For double immunostaining, sections were sequentially incubated with rat anti-CD45R (BD Biosciences – Pharmingen). Immune complexes were detected with HRP-conjugated anti-rat IgG (simple stain Max-Po; Nichirei) and 3-amino-9-ethyl carbazole (AEC) substrate system (Lab Vision) for color development.

S1P release from blood cells. Blood was collected from anesthetized WT (*Spns2*$^{+/+}$, $n = 4$) and *Spns2*$^{-/-}$ (*Spns2*$^{-/-}$, $n = 4$) mice via the inferior vena cava using heparinized syringes and transferred to tubes containing EDTA as an anticoagulant. Blood cells were separated from plasma by centrifugation at 1,200 *g* for 5 minutes at 4°C and washed twice with ice-cold PBS to remove plasma residues. The cells were resuspended in the ice-cold incubation buffer containing 20 mM Hepes, pH 7.4, 138 mM NaCl, 3.3 mM NaH_2PO_4, 2.9 mM KCl, 1.0 mM $MgCl_2$, 1 mg/ml glucose, and 1% fatty acid–free bovine serum albumin at a cell density of 5×10^8 cells/ml. Then 500 μl of blood cell suspensions (2.5×10^8 cells) was incubated at 4°C or at 37°C for 90 minutes. After incubation, the cells were pelleted by centrifugation at 1,200 *g* for 5 minutes at 4°C. The S1P levels in the supernatants were determined as described above. To quantify the total amount of S1P in the blood cells, cells were collected from 500 μl of cell suspensions by centrifugation at 1,200 *g* for 5 minutes at 4°C and homogenized in 100 μl of methanol.

Generation of bone marrow chimeras. Bone marrow chimeras were generated with 5×10^6 freshly isolated total bone marrow cells from femur and tibia of WT and Spns2 floxed mice (donor). Isolated cells were injected i.v. into lethally irradiated (900 cGY) *Spns2*$^{-/-}$ and Spns2-ECKO mice (host). Hematopoietic reconstitution of lymphoid organs of hosts by donor-derived cells was controlled 6 weeks after bone marrow transfer by genotyping of total bone marrow cells. Furthermore, lymphoid organs of reconstituted mice were FACS analyzed as described above.

In situ hybridization and immunohistochemistry on serial tissue sections. In situ hybridization and immunohistochemistry on serial tissue sections was performed by Genostaff. Briefly, the thymus, heart, lung, brain, and kidney of 8-week-old mice were dissected after perfusion, fixed with Tissue Fixative (Genostaff), and then embedded in paraffin by proprietary procedures and sectioned at 6 μm.

For in situ hybridization, tissue sections were de-waxed with xylene and rehydrated through an ethanol series and PBS. The sections were fixed with 4% paraformaldehyde in PBS for 15 minutes and then washed with PBS. The sections were treated with 8 μg/ml Proteinase K in PBS for 30 minutes at 37°C, washed with PBS, refixed with 4% paraformaldehyde in PBS, again washed with PBS, and placed in 0.2 N HCl for 10 minutes. After washing with PBS, the sections were acetylated by incubation in 0.1 M tri-ethanolamine-HCl, pH 8.0, 0.25% acetic anhydride for 10 minutes. After washing with PBS, the sections were dehydrated through a series of ethanol. The cDNA templates for Spns2 were 535-bp and 634-bp fragments corresponding to bases 1629–2163 and 2291–2924 of mouse Spns2 cDNA (GenBank NM_153060.2). Sense and antisense riboprobes for *Spns2* mRNA were synthesized using a digoxigenin RNA labeling kit (Roche) according to the manufacturer's protocol. Hybridization was performed with probes at concentrations of 300 ng/ml in the Probe Diluent-1 (Genostaff) at 60°C for 16 hours. After hybridization, the sections were washed in 5× HybriWash (Genostaff), equal to 5× SSC, at 50°C for 20 minutes and then in 50% formamide, 2× HybriWash at 50°C for 20 minutes, followed by RNase treatment in 50 μg/ml RNase A in 10 mM Tris-HCl, pH 8.0, 1 M NaCl, and 1 mM EDTA for 30 minutes at 37°C. Then the sections were washed twice with 2× HybriWash at 50°C for 20 minutes, twice with 2× HybriWash at 50°C for 20 minutes, and once with TBST (0.1% Tween 20 in TBS). After treatment with 0.5% blocking reagent (Roche) in TBST for 30 minutes, the sections were incubated with anti-DIG AP conjugate (Roche) diluted 1:1,000 with TBST for 2 hours at RT. The sections were washed twice with TBST and then incubated in 100 mM NaCl, 50 mM $MgCl_2$, 0.1% Tween 20, and 100 mM Tris-HCl, pH 9.5. Coloring reactions were performed with NBT/BCIP solution (Sigma-Aldrich) overnight and then washed with PBS. The sections were counterstained with Kernechtrot Stain Solution (Mutoh), dehydrated, and mounted with Malinol (DBS).

For immunohistochemistry, serial tissue sections were deparaffinized with xylene and rehydrated through an ethanol series and TBS. Endogenous peroxidase activity was blocked with 0.3% H_2O_2 in methanol for 30 minutes. For CD31 staining, the sections were treated with Protein Block (Dako) and avidin/biotin blocking kit (Vector), and incubated with 0.1 μg/ml of anti-CD31 rabbit polyclonal antibody (Spring Bioscience) at 4°C overnight. Immune complexes were labeled with biotin-conjugated goat anti-rabbit Ig (Dako) and peroxidase-conjugated streptavidin (Nichirei). For α-SMA staining, sections were treated with Blocking Reagent A (Nichirei) and incubated with anti–α-SMA mouse monoclonal antibody (Dako) at 4°C overnight. The sections were then blocked with Blocking Reagent B (Nichirei) and incubated with Simple Stain Mouse MAX-PO (M) (Nichirei). Peroxidase activity was visualized by diaminobenzidine. The sections were counterstained with Mayer's hematoxylin, dehydrated, and mounted with Malinol (Muto).

Statistics. Data were analyzed using GraphPad Prism software (GraphPad Software Inc.). Statistical significance was determined using a 2-tailed Mann-Whitney *U* test for paired samples or 1-way ANOVA and nonparametric tests for multiple groups. $P < 0.05$ was considered statistically significant.

Study approval. All animal experiments were approved by the animal committee of the National Cerebral and Cardiovascular Center and performed according to the regulations of the National Cerebral and Cardiovascular Center.

Acknowledgments

We thank T.N. Sato and M. Yanagisawa (Nara Institute of Science and Technology and University of Texas Southwestern Medical Center, respectively) for Tie2Cre mice. We are also grateful to K. Hiratomi, W. Koeda, M. Sone, H. Yonekawa, and Y. Matsuura for technical assistance, and to K. Shioya for providing excellent animal facilities. This work was supported in part by Grants-in-Aid for Scientific Research on Innovative Areas, "Fluorescence Live Imaging" (No. 22113009 to S. Fukuhara and No. 22113007 to M. Ishii) and "Neuro-Vascular Wiring" (No. 22122003 to N. Mochizuki), of The Ministry of Education, Culture, Sports, Science, and Technology, Japan; and by grants from the Japan Society for the Promotion of Science (to S. Fukuhara, M. Ishii, and N. Mochizuki); the Ministry of Health, Labour, and Welfare of Japan (to N. Mochizuki); the Program for the Promotion of Fundamental Studies in Health Sciences of the National Institute of Biomedical Innovation (to S. Fukuhara and N. Mochizuki); a grant from the International Human Frontier Science Program (to M. Ishii); the Takeda Science Foundation (to M. Ishii and N. Mochizuki); the Mitsubishi Foundation (to N. Mochizuki); the Japan Cardiovascular Research Foundation (to S. Fukuhara); and an AstraZeneca research grant (to N. Mochizuki).

Received for publication August 30, 2011, and accepted in revised form January 30, 2012.

Address correspondence to: Shigetomo Fukuhara or Naoki Mochizuki, Department of Cell Biology, National Cerebral and Cardiovascular Center Research Institute, 5-7-1 Fujishirodai, Suita, Osaka 565-8565, Japan. Phone: 81.6.6833.5012; Fax: 81.6.6835.5461; E-mail: fuku@ri.ncvc.go.jp (S. Fukuhara), nmochizu@ri.ncvc.go.jp (N. Mochizuki). Or to: Masaru Ishii, Laboratory of Cellular Dynamics, WPI-Immunology Frontier Research Center, Osaka University, 3-1 Yamada-oka, Suita, Osaka 565-0871, Japan. Phone: 81.6.6879.4268; Fax: 81.6.6879.8296; E-mail: mishii@ifrec.osaka-u.ac.jp.

1. Chi H. Sphingosine-1-phosphate and immune regulation: trafficking and beyond. *Trends Pharmacol Sci.* 2011;32(1):16–24.
2. Cyster JG. Chemokines, sphingosine-1-phosphate, and cell migration in secondary lymphoid organs. *Annu Rev Immunol.* 2005;23:127–159.
3. Hla T. Physiological and pathological actions of sphingosine 1-phosphate. *Semin Cell Dev Biol.* 2004; 15(5):513–520.
4. Rivera J, Proia RL, Olivera A. The alliance of sphingosine-1-phosphate and its receptors in immunity. *Nat Rev Immunol.* 2008;8(10):753–763.
5. Spiegel S, Milstien S. The outs and the ins of sphingosine-1-phosphate in immunity. *Nat Rev Immunol.* 2011;11(6):403–415.
6. Alvarez SE, et al. Sphingosine-1-phosphate is a missing cofactor for the E3 ubiquitin ligase TRAF2. *Nature.* 2010;465(7301):1084–1088.
7. Allende ML, Dreier JL, Mandala S, Proia RL. Expression of the sphingosine 1-phosphate receptor, S1P1, on T-cells controls thymic emigration. *J Biol Chem.* 2004;279(15):15396–15401.
8. Matloubian M, et al. Lymphocyte egress from thymus and peripheral lymphoid organs is dependent on S1P receptor 1. *Nature.* 2004;427(6972):355–360.
9. Pappu R, et al. Promotion of lymphocyte egress into blood and lymph by distinct sources of sphingosine-1-phosphate. *Science.* 2007;316(5822):295–298.
10. Schwab SR, Pereira JP, Matloubian M, Xu Y, Huang Y, Cyster JG. Lymphocyte sequestration through S1P lyase inhibition and disruption of S1P gradients. *Science.* 2005;309(5741):1735–1739.
11. Brinkmann V, et al. The immune modulator FTY720 targets sphingosine 1-phosphate receptors. *J Biol Chem.* 2002;277(24):21453–21457.
12. Graler MH, Goetzl EJ. The immunosuppressant FTY720 down-regulates sphingosine 1-phosphate G-protein-coupled receptors. *FASEB J.* 2004; 18(3):551–553.
13. Mandala S, et al. Alteration of lymphocyte trafficking by sphingosine-1-phosphate receptor agonists. *Science.* 2002;296(5566):346–349.
14. Brinkmann V, et al. Fingolimod (FTY720): discovery and development of an oral drug to treat multiple sclerosis. *Nat Rev Drug Discov.* 2010;9(11):883–897.
15. Allende ML, Tuymetova G, Lee BG, Bonifacino E, Wu YP, Proia RL. S1P1 receptor directs the release of immature B cells from bone marrow into blood. *J Exp Med.* 2010;207(5):1113–1124.
16. Pereira JP, Xu Y, Cyster JG. A role for S1P and S1P1 in immature-B cell egress from mouse bone marrow. *PLoS One.* 2010;5(2):e9277.
17. Schwab SR, Cyster JG. Finding a way out: lymphocyte egress from lymphoid organs. *Nat Immunol.* 2007; 8(12):1295–1301.
18. Breart B, et al. Lipid phosphate phosphatase 3 enables efficient thymic egress. *J Exp Med.* 2011; 208(6):1267–1278.
19. Zachariah MA, Cyster JG. Neural crest-derived pericytes promote egress of mature thymocytes at the corticomedullary junction. *Science.* 2010; 328(5982):1129–1135.
20. Pham TH, et al. Lymphatic endothelial cell sphingosine kinase activity is required for lymphocyte egress and lymphatic patterning. *J Exp Med.* 2010; 207(1):17–27.
21. Spiegel S, Milstien S. Functions of the multifaceted family of sphingosine kinases and some close relatives. *J Biol Chem.* 2007;282(4):2125–2129.
22. Kim RH, Takabe K, Milstien S, Spiegel S. Export and functions of sphingosine-1-phosphate. *Biochim Biophys Acta.* 2009;1791(7):692–696.
23. Hanel P, Andreani P, Graler MH. Erythrocytes store and release sphingosine 1-phosphate in blood. *FASEB J.* 2007;21(4):1202–1209.
24. Kobayashi N, et al. Sphingosine 1-phosphate is released from the cytosol of rat platelets in a carrier-mediated manner. *J Lipid Res.* 2006;47(3):614–621.
25. Yang L, Yatomi Y, Miura Y, Satoh K, Ozaki Y. Metabolism and functional effects of sphingolipids in blood cells. *Br J Haematol.* 1999;107(2):282–293.
26. Yatomi Y, et al. Sphingosine 1-phosphate, a bioactive sphingolipid abundantly stored in platelets, is a normal constituent of human plasma and serum. *J Biochem.* 1997;121(5):969–973.
27. Ito K, et al. Lack of sphingosine 1-phosphate-degrading enzymes in erythrocytes. *Biochem Biophys Res Commun.* 2007;357(1):212–217.
28. Olivera A, et al. The sphingosine kinase-sphingosine-1-phosphate axis is a determinant of mast cell function and anaphylaxis. *Immunity.* 2007; 26(3):287–297.
29. Kobayashi N, Kobayashi N, Yamaguchi A, Nishi T. Characterization of the ATP-dependent sphingosine 1-phosphate transporter in rat erythrocytes. *J Biol Chem.* 2009;284(32):21192–21200.
30. Mitra P, Oskeritzian CA, Payne SG, Beaven MA, Milstien S, Spiegel S. Role of ABCC1 in export of sphingosine-1-phosphate from mast cells. *Proc Natl Acad Sci U S A.* 2006;103(44):16394–16399.
31. Sato K, et al. Critical role of ABCA1 transporter in sphingosine 1-phosphate release from astrocytes. *J Neurochem.* 2007;103(6):2610–2619.
32. Takabe K, et al. Estradiol induces export of sphingosine 1-phosphate from breast cancer cells via ABCC1 and ABCG2. *J Biol Chem.* 2010; 285(14):10477–10486.
33. Kawahara A, Nishi T, Hisano Y, Fukui H, Yamaguchi A, Mochizuki N. The sphingolipid transporter spns2 functions in migration of zebrafish myocardial precursors. *Science.* 2009;323(5913):524–527.
34. Osborne N, et al. The spinster homolog, two of hearts, is required for sphingosine 1-phosphate signaling in zebrafish. *Curr Biol.* 2008; 18(23):1882–1888.
35. Campbell JJ, Pan J, Butcher EC. Cutting edge: developmental switches in chemokine responses during T cell maturation. *J Immunol.* 1999;163(5):2353–2357.
36. Weinreich MA, Hogquist KA. Thymic emigration: when and how T cells leave home. *J Immunol.* 2008;181(4):2265–2270.
37. Ge Q, Chen WF. Phenotypic identification of the subgroups of murine T-cell receptor alphabeta+ CD4+ CD8- thymocytes and its implication in the late stage of thymocyte development. *Immunology.* 1999;97(4):665–671.
38. Tian T, Zhang J, Gao L, Qian XP, Chen WF. Heterogeneity within medullary-type TCRαβ$^+$CD3$^+$CD4$^-$CD8$^+$ thymocytes in normal mouse thymus. *Int Immunol.* 2001;13(3):313–320.
39. Rosen H, Alfonso C, Surh CD, McHeyzer-Williams MG. Rapid induction of medullary thymocyte phenotypic maturation and egress inhibition by nanomolar sphingosine 1-phosphate receptor agonist. *Proc Natl Acad Sci U S A.* 2003; 100(19):10907–10912.
40. Argraves KM, Argraves WS. HDL serves as a S1P signaling platform mediating a multitude of cardiovascular effects. *J Lipid Res.* 2007;48(11):2325–2333.
41. Sato K, Okajima F. Role of sphingosine 1-phosphate in anti-atherogenic actions of high-density lipoprotein. *World J Biol Chem.* 2010;1(11):327–337.
42. Aoki S, et al. Sphingosine 1-phosphate-related metabolism in the blood vessel. *J Biochem.* 2005; 138(1):47–55.
43. Lee YM, Venkataraman K, Hwang SI, Han DK, Hla T. A novel method to quantify sphingosine 1-phosphate by immobilized metal affinity chromatography (IMAC). *Prostaglandins Other Lipid Mediat.* 2007;84(3-4):154–162.
44. Venkataraman K, et al. Vascular endothelium as a contributor of plasma sphingosine 1-phosphate. *Circ Res.* 2008;102(6):669–676.
45. Kisanuki YY, Hammer RE, Miyazaki J, Williams SC, Richardson JA, Yanagisawa M. Tie2-Cre transgenic mice: a new model for endothelial cell-lineage analysis in vivo. *Dev Biol.* 2001;230(2):230–242.
46. Schlaeger TM, et al. Uniform vascular-endothelial-cell-specific gene expression in both embryonic and adult transgenic mice. *Proc Natl Acad Sci U S A.* 1997; 94(7):3058–3063.
47. Takakura N, et al. A role for hematopoietic stem cells in promoting angiogenesis. *Cell.* 2000; 102(2):199–209.
48. Liu Y, et al. Edg-1, the G protein-coupled receptor for sphingosine-1-phosphate, is essential for vascular maturation. *J Clin Invest.* 2000;106(8):951–961.
49. Takada K, et al. Kruppel-like factor 2 is required for trafficking but not quiescence in postactivated T cells. *J Immunol.* 2011;186(2):775–783.
50. Nagasawa T. Microenvironmental niches in the bone marrow required for B-cell development. *Nat Rev Immunol.* 2006;6(2):107–116.
51. Osmond DG, Batten SJ. Genesis of B lymphocytes in the bone marrow: extravascular and intravascular localization of surface IgM-bearing cells in mouse bone marrow detected by electron-microscope radioautography after in vivo perfusion of 125I anti-IgM antibody. *Am J Anat.* 1984; 170(3):349–365.
52. Pereira JP, An J, Xu Y, Huang Y, Cyster JG. Cannabinoid receptor 2 mediates the retention of immature B cells in bone marrow sinusoids. *Nat Immunol.* 2009;10(4):403–411.
53. Yagi T, et al. A novel ES cell line, TT2, with high germline-differentiating potency. *Anal Biochem.* 1993; 214(1):70–76.
54. Zhang J, et al. Angiopoietin-1/Tie2 signal augments basal Notch signal controlling vascular quiescence by inducing delta-like 4 expression through AKT-mediated activation of beta-catenin. *J Biol Chem.* 2011;286(10):8055–8066.
55. Fukuhara S, et al. Differential function of Tie2 at cell-cell contacts and cell-substratum contacts regulated by angiopoietin-1. *Nat Cell Biol.* 2008; 10(5):513–526.
56. Inoue A, Arima N, Ishiguro J, Prestwich GD, Arai H, Aoki J. LPA-producing enzyme PA-PLA(1)alpha regulates hair follicle development by modulating EGFR signalling. *EMBO J.* 2011;19(16):4248–4260.
57. Tanaka M, Kishi Y, Takanezawa Y, Kakehi Y, Aoki J, Arai H. Prostatic acid phosphatase degrades lysophosphatidic acid in seminal plasma. *FEBS Lett.* 2004;571(1-3):197–204.

Intestinal CX_3C chemokine receptor 1^{high} (CX_3CR1^{high}) myeloid cells prevent T-cell-dependent colitis

Hisako Kayama[a,b,c], Yoshiyasu Ueda[a,b,c], Yukihisa Sawa[c,d,e], Seong Gyu Jeon[a,b,c], Ji Su Ma[a,b,c], Ryu Okumura[a,b,c], Atsuko Kubo[c,f], Masaru Ishii[c,f], Taku Okazaki[c,g], Masaaki Murakami[c,d,e], Masahiro Yamamoto[a,b,c], Hideo Yagita[h], and Kiyoshi Takeda[a,b,c,1]

[a]Laboratory of Immune Regulation, Department of Microbiology and Immunology, Graduate School of Medicine, Osaka University, Suita, Osaka, 565-0871, Japan; Laboratories of [b]Mucosal Immunology, [e]Developmental Immunology, and [f]Cellular Dynamics, World Premier International Research Center (WPI) Immunology Frontier Research Center, Osaka University, Suita, Osaka, 565-0871, Japan; [c]Core Research for Evolutional Science and Technology, Japan Science and Technology Agency, Saitama, 332-0012, Japan; [d]Laboratory of Developmental Immunology, Graduate School of Frontier Biosciences, Graduate School of Medicine, Osaka University, Suita, Osaka, 565-0871, Japan; [g]Division of Immune Regulation, Institute for Genome Research, University of Tokushima, Tokushima, 770-8503, Japan; and [h]Department of Immunology, Juntendo University School of Medicine, Tokyo, 113-8421, Japan

Edited by Warren Strober, National Institute of Allergy and Infectious Diseases, National Institutes of Health, Bethesda, MD, and accepted by the Editorial Board February 1, 2012 (received for review September 12, 2011)

Adequate activation of $CD4^+$ T lymphocytes is essential for host defense against invading pathogens; however, exaggerated activity of effector $CD4^+$ T cells induces tissue damage, leading to inflammatory disorders such as inflammatory bowel diseases. Several unique subsets of intestinal innate immune cells have been identified. However, the direct involvement of innate immune cell subsets in the suppression of T-cell-dependent intestinal inflammation is poorly understood. Here, we report that intestinal CX_3C chemokine receptor 1^{high} (CX_3CR1^{high}) $CD11b^+$ $CD11c^+$ cells are responsible for prevention of intestinal inflammation through inhibition of T-cell responses. These cells inhibit $CD4^+$ T-cell proliferation in a cell contact-dependent manner and prevent T-cell-dependent colitis. The suppressive activity is abrogated in the absence of the IL-10/Stat3 pathway. These cells inhibit T-cell proliferation by two steps. Initially, CX_3CR1^{high} $CD11b^+$ $CD11c^+$ cells preferentially interact with T cells through highly expressed intercellular adhesion molecule-1/vascular cell adhesion molecule-1; then, they fail to activate T cells because of defective expression of CD80/CD86. The IL-10/Stat3 pathway mediates the reduction of CD80/CD86 expression. Transfer of wild-type CX_3CR1^{high} $CD11b^+$ $CD11c^+$ cells prevents development of colitis in myeloid-specific Stat3-deficient mice. Thus, these cells are regulatory myeloid cells that are responsible for maintaining intestinal homeostasis.

mucosal immunology | innate immunity

Inflammatory bowel diseases (IBDs), represented by Crohn disease and ulcerative colitis in humans, result from genetic abnormalities, as well as uncontrolled intestinal immune responses toward commensal microflora and dietary antigens (1–3). Activation of appropriate mucosal immune responses is responsible for protection against pathogenic microorganisms, whereas excessive immune responses, especially unbalanced T-cell-mediated adaptive immune responses, to commensal microflora and dietary antigens lead to development of intestinal inflammation. Therefore, T-cell-mediated responses are tightly regulated to suppress aberrant inflammatory responses in the intestinal mucosa. Over the last few decades, $CD4^+$ regulatory T (T_{reg}) cells have been demonstrated to prevent T-cell-mediated chronic inflammatory diseases including IBDs (4, 5). Several possible mechanisms for this suppressive effect of T_{reg} cells have been proposed. Regulatory dendritic cells have also been implicated in the immune tolerance by inducing T_{reg} cells (6, 7). In tumor models, myeloid-derived suppressor cells (MDSCs) have been reported to suppress T-cell-mediated responses through several mechanisms (8, 9).

Several subsets of intestinal innate phagocytic cells have recently been identified that modulate intestinal homeostasis (10–12). In particular, $CD103^+$ CX_3CR1^- $CD11b^-$ dendritic cells (DCs) and CX_3CR1^+ $CD11b^+$ DCs have been well characterized (13–15). $CD103^+$ CX_3CR1^- $CD11b^-$ DCs have been shown to generate and activate gut-tropic $CD8^+$ T cells (16, 17). These DCs have further been shown to induce development of $Foxp3^+$ T_{reg} cells (18–20). CX_3CR1^+ $CD11b^+$ DCs have been shown to mediate inflammatory responses through the induction of Th1 and Th17 cell development (15, 21–24). In addition to these cell populations, $CD103^+$ CX_3CR1^- $CD11b^+$ cells and $CD11b^+CD11c^-$ macrophages have been identified in the intestinal lamina propria (13, 14, 22, 25). Other intestinal myeloid cell populations inducing T_{reg} cells have also been characterized (26–28). However, it remains unclear whether cell populations other than T_{reg} cells directly contribute to the suppression of inflammatory responses.

In this study, we characterized intestinal CX_3C chemokine receptor 1^{high} (CX_3CR1^{high}) $CD11b^+$ $CD11c^+$ cells, which show a cell contact-dependent suppression of T-cell proliferation, leading to prevention of intestinal inflammation.

Results

Intestinal CX_3CR1^{high} $CD11b^+$ $CD11c^+$ Cells Suppress T-Cell Growth. Several unique subsets of innate immune cells in the intestinal lamina propria have been identified (12–14, 16–26, 28–30). Among these subsets, $CD103^+$ CX_3CR1^- $CD11b^-$ $CD11c^+$ cells and CX_3CR1^+ $CD11b^+$ $CD11c^+$ cells have been reported to be major subsets in the intestine (13, 14). The functions of CX_3CR1^+ $CD11b^+$ $CD11c^+$ cells have been characterized in several aspects (13, 14, 17). However, the $CD11b^+$ $CD11c^+$ cell population could be divided into three subsets based on the expression level of CX_3CR1: CX_3CR1^{high}, $CX_3CR1^{intermediate\ (int)}$, and $CX_3CR1^{negative\ (-)}$ cells (Fig. S1A) (13, 17). Although previous studies have indicated the presence of CX_3CR1^{high} and CX_3CR1^{int} cells, differential functions of these cell subsets in T-cell differentiation have not been characterized (13, 17). Therefore, we examined the effects of three subsets on induction of Th1, Th17, and T_{reg} cells (Fig. 1A). CX_3CR1^{high}, CX_3CR1^{int}, and CX_3CR1^- cells were isolated from the colonic lamina propria and cultured with splenic naïve $CD4^+$ T cells for 4 d. $CD4^+$ T cells cocultured with CX_3CR1^{int} or CX_3CR1^- cells predominantly produced IL-17 or IFN-γ,

Author contributions: H.K. and K.T. designed research; H.K., Y.U., S.G.J., J.S.M., and R.O. performed research; Y.S., A.K., M.I., T.O., M.M., M.Y., and H.Y. contributed new reagents/analytic tools; H.K., Y.S., S.G.J., J.S.M., M.I., M.M., and K.T. analyzed data; and H.K. and K.T. wrote the paper.

The authors declare no conflict of interest.

This article is a PNAS Direct Submission. W.S. is a guest editor invited by the Editorial Board.

[1]To whom correspondence should be addressed. E-mail: ktakeda@ongene.med.osaka-u.ac.jp.

This article contains supporting information online at www.pnas.org/lookup/suppl/doi:10.1073/pnas.1114931109/-/DCSupplemental.

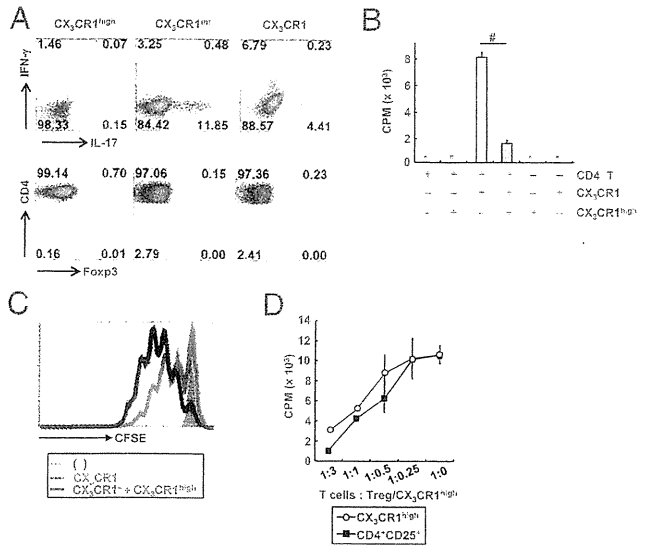

Fig. 1. CX_3CR1^{high} $CD11b^+$ $CD11c^+$ cells in the intestinal lamina propria suppress T-cell proliferation. (*A*) Flow cytometric plots of IL-17-, IFN-γ-, or Foxp3-expressing $CD4^+$ T cells cocultured with the indicated cells for 72 h. (*B*) [^{3}H]thymidine uptake of $CD4^+$ T cells cultured with the indicated cells. #$P <$ 0.022. (*C*) The fluorescence intensity of CFSE-labeled $CD4^+$ T cells cultured with the indicated cells at a ratio 1:1:1 for 72 h. (*D*) [^{3}H]thymidine uptake by $CD4^+$ T cells cocultured with CX_3CR1^- DCs in the presence of increasing ratios of splenic $CD4^+$ $CD25^+$ T_{reg} cells (closed rectangle) or colonic CX_3CR1^{high} cells (open circle). All data are representative of two independent experiments (means ± SD of duplicate well measurements).

respectively. In contrast, expression of IFN-γ, IL-17, or Foxp3 was not induced in $CD4^+$ T cells cocultured with the CX_3CR1^{high} cells. Next, we examined the effects on T-cell proliferation. $CD4^+$ T cells were cocultured with the CX_3CR1^{high}, CX_3CR1^{int}, or CX_3CR1^- cells for 72 h, and their proliferation was analyzed by assessing incorporation of [^{3}H]thymidine (Fig. S1*B*). $CD4^+$ T cells cocultured with CX_3CR1^- and CX_3CR1^{int} cells showed robust proliferative responses, indicating that the CX_3CR1^- and CX_3CR1^{int} cells had similar properties as DCs in enhancing T-cell responses. In contrast, $CD4^+$ T cells cocultured with CX_3CR1^{high} cells did not show any enhanced proliferation. These findings indicate that CX_3CR1^{high} cells are not typical DCs. Indeed, CX_3CR1^{high} cells express several macrophage-related molecules (CD14, CD68, and F4/80), as well as DC-related molecules (CD11c and DEC205) (Fig. S1*C*). In addition, CX_3CR1^{high} cells contain cytoplasmic vacuolar structures characteristic of macrophages (Fig. S1*D*) (14). We further found that the addition of CX_3CR1^{high} cells into a coculture of $CD4^+$ T cells and CX_3CR1^- DCs profoundly reduced T-cell proliferation (Fig. 1*B*). The suppression of T-cell proliferation by the CX_3CR1^{high} cells was further confirmed by reduced dilution of the fluorescence intensity of $CD4^+$ T cells labeled with carboxyfluorescein succinimidyl ester (CFSE) (Fig. 1*C*). We then compared the suppressive ability of CX_3CR1^{high} cells on T-cell proliferation with that of T_{reg} cells. $CD4^+$ T cells were cultured with DCs and anti-CD3 mAb in the presence of various numbers of T_{reg} cells or CX_3CR1^{high} cells (Fig. 1*D*). The CX_3CR1^{high} cells showed a dose-dependent suppression of T-cell proliferation in a very similar manner to that induced by T_{reg} cells. CX_3CR1^{high} cells isolated from $CX_3CR1^{+/GFP}$ mice, in which CX_3CR1 Ab staining was well correlated with GFP expression (Fig. S1*E*), also inhibited T-cell proliferation (Fig. S1*F*). CX_3CR1^{high} cells were not present in the $CD11b^+$ $CD11c^+$ population in the spleen, mesenteric lymph nodes (MLNs), or thymus (Fig. S1*G*). Collectively, our in vitro analyses suggested that a CX_3CR1^{high} $CD11b^+$ $CD11c^+$ subset of intestinal myeloid cells inhibited T-cell proliferation independently of T_{reg} induction.

CX_3CR1^{high} Myeloid Cells Prevent Intestinal Inflammation. We next assessed the in vivo function of the CX_3CR1^{high} subset of intestinal myeloid cells using a T-cell-dependent colitis model. Severe combined immunodeficiency (SCID) mice given $CD45RB^{high}$ $CD4^+$ T cells showed severe weight loss with severe intestinal pathology (Fig. 2 *A* and *B*). Cotransfer of CX_3CR1^{high} cells dramatically reduced their weight loss and the severity of intestinal inflammation. The cotransfer of CX_3CR1^{high} cells did not induce any change in the frequency of IL-17-, IFN-γ-, IL-4-, or IL-10-producing $CD4^+$ T cells or in the frequency of Foxp3-expressing $CD4^+$ T cells in the colonic lamina propria (Fig. S2). However, the total number of $CD4^+$ T cells in the lamina propria was markedly reduced by CX_3CR1^{high} cell coadministration (Fig. 2*C*). Assessment of CFSE dilution in transferred $CD45RB^{high}$ $CD4^+$ T cells demonstrated robust T-cell proliferation in the colonic lamina propria of $Rag2^{-/-}$ mice. However, cotransfer of CX_3CR1^{high} cells substantially inhibited CFSE dilution in transferred T cells (Fig. 2*D*). Transferred CX_3CR1^{high} cells were observed just beneath the epithelial cell layers of the intestine but

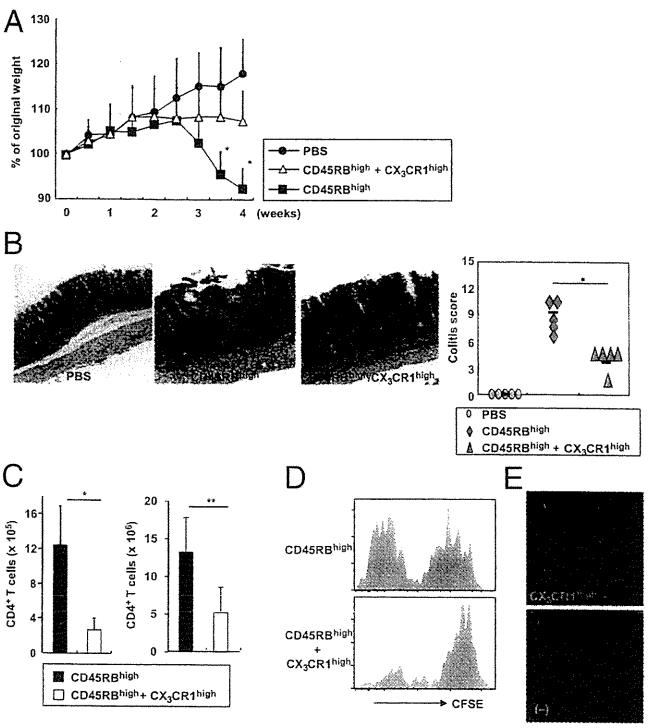

Fig. 2. CX_3CR1^{high} myeloid cells alleviate T-cell-dependent intestinal inflammation. (*A*) SCID mice were injected i.p. with 3×10^5 $CD45RB^{high}$ $CD4^+$ T cells or PBS (closed circles). After 2 h, 3×10^5 CX_3CR1^{high} cells were transferred (open triangles) or not (closed rectangles). Body weight change was monitored and is presented relative to initial body weight. *$P < 0.005$ ($n = 8$ per group). (*B*) Hematoxylin and eosin staining of colon sections at 4 wk after the transfer described in *A* (*Left*) and the colitis score (*Right*). *$P <$ 0.0012. (Original magnification, 200×.) (*C*) Numbers of large intestinal lamina propria $CD4^+$ T cells at 2 wk ($n = 4$ per group) (*Left*) and 4 wk ($n = 5$ per group) (*Right*) after transfer. *$P < 0.02$; **$P < 0.015$. (*D*) $CD45RB^{high}$ T cells (3×10^5) were labeled with CFSE and transferred into $Rag2^{-/-}$ mice with or without 3×10^5 CX_3CR1^{high} cells. After 12 d, CFSE dilution in colonic $CD4^+$ T cells was analyzed. (*E*) Cryosection of the colon from a SCID mouse at 3 d after i.v. injection of CFSE-labeled CX_3CR1^{high} cells. (Original magnification, 200×.) Data are representative of three independent experiments (*D* and *E*).

not in MLNs or spleen (Fig. 2*E* and Fig. S3 *A* and *B*). Transferred CX_3CR1^{high} cells were in close proximity to T cells in the lamina propria (Fig. S3*C*). In addition, the number of $CD4^+$ T cells was reduced where CX_3CR1^{high} cells were present (Fig. S3 *C* and *D*). Total number of CX_3CR1^{high} cells increased in the colonic lamina propria of the transferred mice (Fig. S4). Thus, the CX_3CR1^{high} subset of intestinal myeloid cells suppresses T-cell proliferation in the intestinal lamina propria, thereby preventing intestinal inflammation; hereafter, we call this subset CX_3CR1^{high} regulatory myeloid (M_{reg}) cells.

IL-10/Stat3-Dependent Suppressive Ability of CX_3CR1^{high} M_{reg} Cells. To determine how CX_3CR1^{high} M_{reg} cells exert their immunosuppressive function, we performed a comprehensive analysis of gene expression profiles in CX_3CR1^{high} M_{reg} cells. CX_3CR1^{high} M_{reg} cells expressed several IL-10-inducible genes such as *Hpgd*, *Cd163*, *Hmox1*, *Cd209f*, and *Cd209g* (Fig. S5*A*). Hence, we analyzed CX_3CR1^{high} M_{reg} cells in $Il10^{-/-}$ mice. Because normal numbers of CX_3CR1^{high} M_{reg} cells were observed in the colon of $Il10^{-/-}$ mice (Fig. S5*B*), we isolated these cells and analyzed the expression of the genes that were selectively expressed in wild-type CX_3CR1^{high} M_{reg} cells. Expression of *Hpgd*, *Cd163*, *Hmox1*, *Cd209f*, and *Cd209g* was severely decreased in $Il10^{-/-}$ cells despite normal expression of the myeloid cell-related gene *Cebpb* (Fig. 3*A*). CX_3CR1^{high} M_{reg} cells from LysM-*cre*; $Stat3^{fl/fl}$ mice ($Stat3^{-/-}$ CX_3CR1^{high} M_{reg} cells) also showed profoundly decreased levels of expression of these genes (Fig. 3*B*). To evaluate whether $Stat3^{-/-}$ CX_3CR1^{high} M_{reg} cells suppress the T-cell proliferative response, wild-type or $Stat3^{-/-}$ CX_3CR1^{high} M_{reg} cells were added to coculture of $CD4^+$ T cells with wild-type DCs (Fig. 3*C*). $Stat3^{-/-}$ CX_3CR1^{high} M_{reg} cells were not able to suppress T-cell proliferation. $Il10^{-/-}$ CX_3CR1^{high} M_{reg} cells were also defective in their suppression of T-cell proliferation (Fig. 4*E*). Furthermore, $Stat3^{-/-}$ CX_3CR1^{high} M_{reg} cells showed impaired prevention of intestinal inflammation in $Rag2^{-/-}$ mice given $CD45RB^{high}$ $CD4^+$ T cells (Fig. 3*D*). Thus, the suppressive function of CX_3CR1^{high} M_{reg} cells in vitro and in vivo was impaired in the absence of IL-10/Stat3 signaling.

CX_3CR1^{high} M_{reg} Cells Inhibit T-Cell Growth by Two Steps. We then assessed the mechanism underlying the suppression of T-cell proliferation by CX_3CR1^{high} M_{reg} cells. Because MDSCs have been reported to suppress T-cell response through arginase-1, inducible NOS, and reactive oxygen species (ROS) (8, 9), we analyzed the effects of inhibitors of these mediators. However, the inhibitors did not cancel the suppressive activity of CX_3CR1^{high} M_{reg} cells (Fig. S6 *A*–*E*). Expression of indoleamine 2, 3-dioxygenase (IDO) in several regulatory DCs inhibits T-cell responses (6, 20). However, T-cell proliferation was not increased by addition of an IDO inhibitor (Fig. S6*F*). Moreover, CX_3CR1^{high} M_{reg} cells did not express T_{reg}-related genes such as *Foxp3*, *Ctla4*, and *Folr4* (Fig. S6*G*). Thus, CX_3CR1^{high} M_{reg} cells possess distinct mechanisms from those used by those cells previously shown to inhibit T-cell proliferation. Coculture of CX_3CR1^{high} M_{reg} cells with $CD4^+$ T cells in transwell plates did not suppress T-cell proliferation, indicating that cell–cell contact is required for suppression (Fig. S6*H*). Addition of CX_3CR1^{high} M_{reg} cells to cocultures of $CD4^+$ T cells and DCs substantially decreased T-cell aggregation around DCs; instead, T cells preferentially associated with CX_3CR1^{high} M_{reg} cells (Fig. 4*A*). Inhibition of T-cell aggregation was not observed in $Stat3^{-/-}$ and $Il10^{-/-}$ CX_3CR1^{high} M_{reg} cells. Thus, CX_3CR1^{high} M_{reg} cells had a higher affinity to interact with T cells than DCs and, thereby, suppressed T-cell responses. These findings prompted us to investigate the expression of adhesion molecules that are involved in DC–T-cell interactions. Surface expression of intercellular adhesion molecule (ICAM)-1, ICAM-2, lymphocyte function-associated antigen (LFA)-1, and vascular cell adhesion molecule (VCAM)-1 was considerably higher in CX_3CR1^{high} M_{reg} cells than in CX_3CR1^- DCs (Fig. 4*B*). Therefore, we analyzed whether these adhesion molecules are involved in the CX_3CR1^{high} M_{reg} suppressive activity. Treatment of CX_3CR1^{high} M_{reg} cells with blocking mAbs to ICAM-1, ICAM-2, LFA-1, and VCAM-1 canceled the CX_3CR1^{high} M_{reg} suppressive activity on T-cell proliferation (Fig. 4*C*). Treatment of CX_3CR1^{high} M_{reg} cells with each mAb did not abrogate the suppressive activity (Fig. S7*A*), but the combination of ICAM-1 and VCAM-1 mAbs substantially induced T-cell proliferation. In addition, treatment of CX_3CR1^{high} M_{reg} cells with mAbs to ICAM-1 and VCAM-1 resulted in increased aggregation of $CD4^+$ T cells around DCs (Fig. 4*D*). These results indicate that an ICAM-1/VCAM-1-mediated interaction is required for suppression. Expression of ICAM-1 and VCAM-1 was high in $Stat3^{-/-}$ and $Il10^{-/-}$ CX_3CR1^{high} M_{reg} cells, which showed impaired suppressive activity (Fig. 4*B* and Fig. S7*B*). In addition, T cells aggregated around $Stat3^{-/-}$ and $Il10^{-/-}$ CX_3CR1^{high} M_{reg} cells (Fig. 4*A*). Therefore, we analyzed how

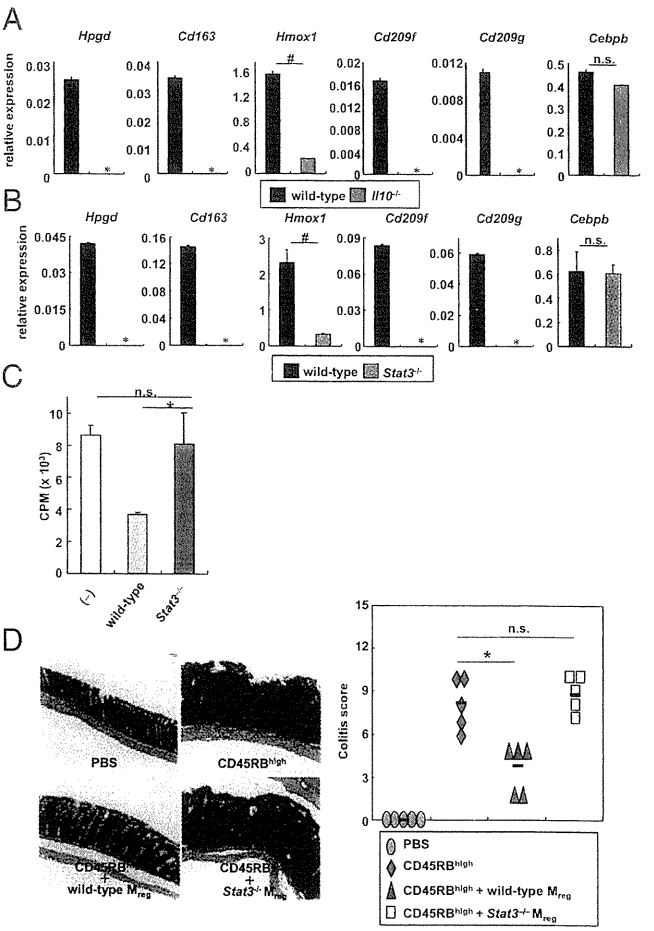

Fig. 3. Defective activity of $Stat3^{-/-}$ M_{reg} cells. (*A* and *B*) Expression of *Hpgd*, *Cd163*, *Hmox1*, *CD209f*, *CD209g*, and *Cebpb* mRNA in CX_3CR1^{high} M_{reg} cells from wild-type, $Il10^{-/-}$, and LysM-*cre*; $Stat3^{fl/fl}$ mice. Data are presentative of two independent experiments (means ± SD of at least triplicate PCRs on the identical sample). *, not detected; #$P < 0.025$. (*C*) [^{3}H]thymidine uptake by $CD4^+$ T cells cultured with CX_3CR1^- DCs in the presence of wild-type or $Stat3^{-/-}$ CX_3CR1^{high} M_{reg} cells. Data are representative of four independent experiments (means ± SD of triplicate well measurements). *$P < 0.047$. (*D*) Hematoxylin and eosin staining of colon sections of $Rag2^{-/-}$ mice given 3×10^5 $CD45RB^{high}$ $CD4^+$ T cells with 3×10^5 M_{reg} cells from wild-type or LysM-*cre*; $Stat3^{fl/fl}$ mice (*Left*) and colitis score (*Right*). (Original magnification, 200×.) *$P < 0.025$ ($n = 5$ per group).

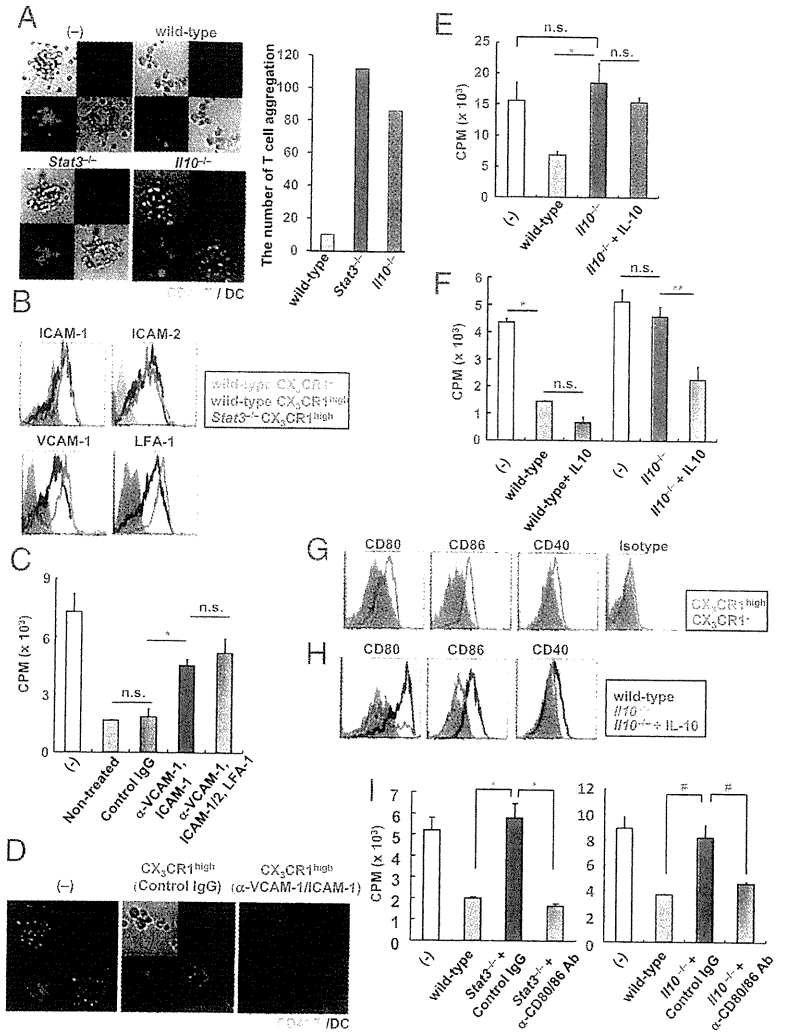

Fig. 4. Two-step mechanism for suppression of T-cell growth by M_{reg} cells. (*A*) Green dye-labeled $CD4^+$ T cells were cultured with nonlabeled CX_3CR1^- DCs and red dye-labeled M_{reg} cells from wild-type, LysM-*cre*; *Stat3*$^{fl/fl}$, or *Il10*$^{-/-}$ mice (*Left*). The number of T-cell aggregation in twenty fields (*Right*). (Original magnification, 100×.) (*B*) Expression of adhesion molecules on the indicated cells from wild-type and LysM-*cre*; *Stat3*$^{fl/fl}$ mice. (*C*) $CD4^+$ T cells and wild-type CX_3CR1^- DCs were cocultured with M_{reg} cells pretreated with the indicated blocking Abs or control Ig for evaluation of T-cell proliferation. $^*P < 0.012$. (*D*) Red dye-labeled CX_3CR1^{high} M_{reg} cells were treated with blocking Abs to ICAM-1 and VCAM-1 then added to the mixture of green dye-labeled $CD4^+$ T cells and nonstained CX_3CR1^- DCs. (Original magnification, 100×.) (*E*) IL-10 (100 ng/mL) was added to the coculture of $CD4^+$ T cells, wild-type DCs, and *Il10*$^{-/-}$ M_{reg} cells. Then, T-cell proliferation was measured. $^*P < 0.02$. (*F*) Wild-type and *Il10*$^{-/-}$ M_{reg} cells were preincubated with or without 100 ng/mL IL-10 for 72 h. Then, the cells were analyzed for the suppressive activity of T-cell proliferation. $^*P < 0.016$; $^{**}P < 0.034$. (*G*) Surface expression of CD80, CD86, CD40, and MHC class II on CX_3CR1^{high} M_{reg} cells and CX_3CR1^- DCs. (*H*) Expression of CD80, CD86, and CD40 on M_{reg} cells from wild-type and *Il10*$^{-/-}$ mice cultured for 48 h with or without 100 ng/mL IL-10. (*I*) *Stat3*$^{-/-}$ and *Il10*$^{-/-}$ M_{reg} cells were pretreated with the indicated blocking Abs. Then, M_{reg} cells were cultured with $CD4^+$ T cells and wild-type CX_3CR1^- DCs, and T-cell proliferation was measured. $^*P < 0.025$; $^{\#}P < 0.045$. All data are representative of at least two independent experiments (mean values ± SD of triplicate well measurements).

CX_3CR1^{high} M_{reg} cells with high affinity for T cells show IL-10-dependent suppression of T-cell proliferation. CX_3CR1^{high} M_{reg} cells produced IL-10 constitutively (Fig. S8 *A* and *B*). However, supplementation of exogenous IL-10 into cocultures of $CD4^+$ T cells and *Il10*$^{-/-}$ CX_3CR1^{high} M_{reg} cells did not induce the reduction of T-cell proliferative responses (Fig. 4*E*). In addition, the suppressive activity of wild-type CX_3CR1^{high} M_{reg} cells was not blocked in the presence of neutralizing Abs to IL-10 and the IL-10 receptor (Fig. S8*C*). Thus, IL-10 is not directly involved in the suppression of T-cell proliferation. However, IL-10 pretreatment of *Il10*$^{-/-}$, but not *Stat3*$^{-/-}$, CX_3CR1^{high} M_{reg} cells before coculture led to a substantial reduction of T-cell proliferative responses, indicating that IL-10 provides a key signal for CX_3CR1^{high} M_{reg} cells to acquire suppressive activity (Fig. 4*F* and Fig. S8*D*). Expression of molecules that transduce coinhibitory signals toward T cells, including B7-H4, herpesvirus entry mediator (HVEM), programmed death ligand (PD-L)1, and PD-L2 was increased in CX_3CR1^{high} M_{reg} cells compared with CX_3CR1^- DCs (Fig. S8*E*). However, expression of these coinhibitory molecules remained high in *Stat3*$^{-/-}$ CX_3CR1^{high} M_{reg} cells. Furthermore, the possible involvement of these inhibitory molecules in the suppressive activity of CX_3CR1^{high} M_{reg} cells was ruled out in experiments using neutralizing Abs and knockout mice (Fig. S8 *F*–*H*). In contrast, expression of CD80 and CD86 was severely decreased in CX_3CR1^{high} M_{reg} cells compared with that in CX_3CR1^- DCs, although MHC class II was equally and highly expressed in both populations (Fig. 4*G* and Fig. S8*C*). Notably, expression of CD80 and CD86 was considerably higher in *Il10*$^{-/-}$ and *Stat3*$^{-/-}$ CX_3CR1^{high} M_{reg} cells than in wild-type CX_3CR1^{high} M_{reg} cells (Fig. 4*H* and Fig. S9*A*). Furthermore, IL-10 treatment of *Il10*$^{-/-}$ CX_3CR1^{high} M_{reg} cells decreased the expression of CD80 and CD86 (Fig. 4*H*). Therefore, we suspected that CX_3CR1^{high} M_{reg} cells with decreased expression of costimulatory molecules compete with DCs to suppress T-cell proliferation. To test this, *Stat3*$^{-/-}$ and *Il10*$^{-/-}$ CX_3CR1^{high} M_{reg} cells were pretreated with blocking mAbs to CD80 and CD86, and then cocultured with $CD4^+$ T cells (Fig. 4*I*). *Stat3*$^{-/-}$ and *Il10*$^{-/-}$ CX_3CR1^{high} M_{reg} cells pretreated with mAbs to CD80 and CD86 suppressed T-cell proliferation. These findings clearly indicate that CX_3CR1^{high} M_{reg} cells suppress T-cell responses via a two-step mechanism: CX_3CR1^{high} M_{reg} cells interact with T cells with high affinity through high expression of adhesion molecules and then show IL-10-dependent suppression of CD80/CD86-mediated costimulatory signals, leading to inhibition of T-cell proliferation.

Defective CX_3CR1^{high} M_{reg} Function Results in Development of Colitis. The aberrant Th1/Th17-mediated responses attributable to enhanced DC activity have been considered to induce intestinal inflammation in *Il10*$^{-/-}$ mice and innate immune cell-specific Stat3 mutant mice (31–34). Because the function of CX_3CR1^{high} M_{reg} cells was impaired in the absence of IL-10/Stat3, we assessed

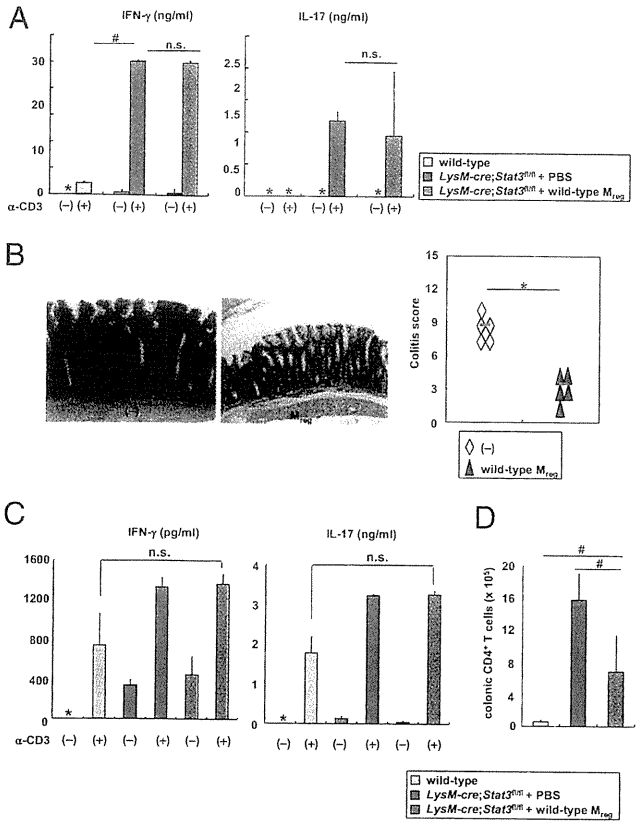

Fig. 5. Defective M_{reg} cell function leads to development of colitis. (*A*, *C*, and *D*) LysM-*cre*; *Stat3*$^{fl/fl}$ mice were transferred i.p. with 7×10^4 wild-type CX_3CR1^{high} M_{reg} cells at 4 and 6 wk of age. At 2 wk after the last transfer, splenic (*A*) or colonic lamina propria (*C*) $CD4^+$ T cells were analyzed for production of IFN-γ and IL-17A. *, not detected; $^{\#}P < 0.008$. Total number of $CD4^+$ T cells in the colonic lamina propria was analyzed (*D*). $^{\#}P < 0.0079$. Data are from two independent experiments with four mice per group. (*B*) Hematoxylin and eosin staining of colon sections at 2 wk after the last transfer (*Left*) and the colitis score (*Right*). (Original magnification, 200×.) $^*P < 0.0002$.

the involvement of CX_3CR1^{high} M_{reg} cells in the pathogenesis of intestinal inflammation in LysM-*cre*; *Stat3*$^{fl/fl}$ mice. LysM-*cre*; *Stat3*$^{fl/fl}$ mice were transferred with wild-type CX_3CR1^{high} M_{reg} cells and were analyzed for Th1 and Th17 activities. In LysM-*cre*; *Stat3*$^{fl/fl}$ mice, Th1 and Th17 activities, as determined by IFN-γ and IL-17A production from splenic $CD4^+$ T cells, respectively, were increased (Fig. 5*A*). Even in LysM-*cre*; *Stat3*$^{fl/fl}$ mice transferred with wild-type CX_3CR1^{high} M_{reg} cells, Th1 and Th17 activity remained considerably enhanced. However, the severity of intestinal inflammation was greatly improved in LysM-*cre*; *Stat3*$^{fl/fl}$ mice transferred with wild-type CX_3CR1^{high} M_{reg} cells (Fig. 5*B*). $CD4^+$ T cells in the colonic lamina propria produced increased amounts of IFN-γ and IL-17A even in LysM-*cre*; *Stat3*$^{fl/fl}$ mice transferred with wild-type CX_3CR1^{high} M_{reg} cells; however, the total number of $CD4^+$ T cells was markedly decreased in the lamina propria (Fig. 5 *C* and *D*). These findings demonstrate that the defective activity of CX_3CR1^{high} M_{reg} cells is critically involved in the development of spontaneous colitis when T cells are overactivated and that transfer of normal CX_3CR1^{high} M_{reg} cells is able to ameliorate the colitis.

Discussion

In the present study, we characterized the intestinal CX_3CR1^{high} $CD11b^+$ $CD11c^+$ M_{reg} cell subset, which directly inhibits T-cell proliferation and, thereby, prevents T-cell-dependent intestinal inflammation. The IL-10/Stat3 pathway is critically involved in the suppressive activity of CX_3CR1^{high} M_{reg} cells.

To date, $CD103^+$ CX_3CR1^- DCs and CX_3CR1^+ $CD11b^+$ $CD11c^+$ cells have been identified as major DC subsets in the intestine. Previous studies indicated that intestinal CX_3CR1^+ $CD11b^+$ $CD11c^+$ cells are further divided into two subsets based on the expression level of CX_3CR1, but these studies did not analyze differential functions of CX_3CR1^{high} and CX_3CR1^{int} cells (13, 17). This study clearly demonstrates that CX_3CR1^{high} $CD11b^+$ $CD11c^+$ cells are a regulatory myeloid cell subset possessing unique functions that directly suppress T-cell proliferation. Previous studies indicated that CX_3CR1^+ $CD11b^+$ $CD11c^+$ cells mediate inflammatory responses such as Th17 cell induction (21–23). In this regard, when splenic naïve $CD4^+$ T cells were cocultured with unsorted CX_3CR1^+ $CD11b^+$ $CD11c^+$ cells, including CX_3CR1^{high} and CX_3CR1^{int} cells, T cells did not vigorously proliferate, although they produced IL-17. In contrast, splenic naïve $CD4^+$ T cells cocultured with CX_3CR1^{int} subset robustly proliferated and produced higher amounts of IL-17 compared with T cells cocultured with unsorted CX_3CR1^+ $CD11b^+$ $CD11c^+$ cells (Fig. S9*B*). These observations would be attributable to suppression of T-cell proliferation by CX_3CR1^{high} M_{reg} cells present within the CX_3CR1^+ $CD11b^+$ $CD11c^+$ cell population. Thus, CX_3CR1^{high} and CX_3CR1^{int} cells are shown to possess distinct functions suppressing and activating T cells, respectively. At present, these functionally distinct populations can only be separated by expression level of CX_3CR1, indicating that both populations are related. It is possible that CX_3CR1^{int} cells are precursors of CX_3CR1^{high} cells, and both cell populations show plasticity. Several previous reports have shown that CX_3CR1^+ cells have macrophage-like properties (14, 15, 35, 36). Indeed, CX_3CR1^{high} M_{reg} cells show macrophage-like morphology and express macrophage-related surface markers. On the other hand, we found that *Stat3*$^{-/-}$ and *Il10*$^{-/-}$ CX_3CR1^{high} M_{reg} cells induced T-cell proliferation, indicating that CX_3CR1^{high} M_{reg} cells show DC-like properties in the absence of the IL-10/Stat3 signaling in vitro (Fig. S9*C*). Therefore, it is possible that CX_3CR1^{int} cells are precursors of CX_3CR1^{high} cells and terminally differentiate into CX_3CR1^{high} M_{reg} cells sharing some macrophage-like properties in response to IL-10.

Several regulatory subsets of myeloid cells, which might be related to M_{reg} cells, have been reported. Colonic IL-10-producing $F4/80^+$ $CD11b^+$ myeloid cells have been reported to mediate the maintenance of Foxp3 expression in T_{reg} cells (26). This subset is observed in MLNs, where M_{reg} cells are not present. Intestinal macrophages suppress T-cell responses via IL-10-dependent induction of T_{reg} cells (22). Unlike M_{reg} cells, these macrophages do not express CD11c, CD14, or DEC205. Most recently, the activity of intestinal macrophages has been shown to be regulated by CX_3CR1 (37). Indeed, mice deficient in CX_3CR1 were highly sensitive to intestinal inflammation induced by dextran sodium sulfate. These intestinal cells might include CX_3CR1^{high} M_{reg} cells. It is interesting to analyze the suppressive activity of CX_3CR1^{high} M_{reg} cells in CX_3CR1-deficient mice. MDSCs are also the cell population similar to CX_3CR1^{high} M_{reg} cells. However, MDSCs do not express CD11c or MHC class II and are hardly detected in healthy mice (9, 38), whereas CX_3CR1^{high} M_{reg} cells express CD11c and MHC class II and are abundant in the intestinal lamina propria of healthy mice. Expression of CX_3CR1^{high} M_{reg} cell-related genes (*Hpgd*, *Cd163*, *Hmox1*, *Cd209f*, and *Cd209g*) was severely reduced in MDSCs, whereas MDSC-related genes (*Arg1*, *Nos2*, *Cybb*, *S100a8*, and *S100a9*) were not expressed in CX_3CR1^{high} M_{reg} cells (Fig. S9 *D* and *E*).

$CD103^+$ CX_3CR1^- DCs have been shown to promote intestinal immune tolerance through the generation of $Foxp3^+$ T_{reg} cells (15, 16, 18, 19). Intestinal macrophages are also reported to induce $Foxp3^+$ T_{reg} cells (22). Intestinal epithelial cells have been implicated in promoting differentiation of $CD103^+$ DCs possessing

a property to induce T_{reg} cells (39, 40). CX_3CR1^{high} M_{reg} cells localize very close to intestinal epithelial cells. Therefore, intestinal epithelial cells might be involved in the final maturation (or differentiation) of CX_3CR1^{high} M_{reg} cells in the intestinal lamina propria through modulation of IL-10 production.

In the present study, we characterize intestinal CX_3CR1^{high} $CD11b^+$ $CD11c^+$ cells (CX_3CR1^{high} M_{reg} cells) that suppress intestinal inflammation through direct inhibition of T-cell proliferation in the intestinal lamina propria. T_{reg} cells with a normal suppressive activity are abundantly present in LysM-cre/$Stat3^{f/f}$ mice (33), indicating that defective activity of CX_3CR1^{high} M_{reg} cells can cause intestinal inflammation even in the presence of T_{reg} cells. Therefore, CX_3CR1^{high} M_{reg} cells maintain the intestinal homeostasis together with T_{reg} cells, as well as several innate cell subsets that have regulatory functions. Identification of an CX_3CR1^{high} M_{reg} population in the human intestines and characterization of human CX_3CR1^{high} M_{reg} function in patients with IBD will be a critical future issue in establishing their role in the pathogenesis of intestinal inflammation in humans.

Materials and Methods

Mice. C57BL/6J mice and BALB/c mice at 6–8 wk of age were purchased from CLEA Japan or Japan SLC. Male 6-wk-old CB17-SCID mice were purchased from CLEA Japan. LysM-*cre*; *Stat3*$^{fl/fl}$ mice and CX_3CR1-EGFP knock-in (heterozygous) mice were generated as described (32, 41, 42). *Il10*$^{-/-}$ mice were purchased from The Jackson Laboratory. Each mutant mouse strain was backcrossed onto a C57BL/6J background for at least five generations. All animal experiments were conducted in accordance with the guidelines of the Animal Care and Use Committee of Osaka University.

The details of reagents, isolation of lamina propria cells, histopathological score, and proliferation assay are described in *SI Materials and Methods*.

ACKNOWLEDGMENTS. We thank S. Sakaguchi and T. Hirano for fruitful discussions; C. Hidaka for secretarial assistance; E. Morii for histological analysis; J. Kikuta and E. Ohata for microscopy analysis; and K. Atarashi, D. Dodd, and Y. Magota for technical assistance. This work was supported by a grant-in-aid from the Ministry of Education, Culture, Sports, Science and Technology; the Ministry of Health, Labour and Welfare; The Kato Memorial Trust for Nambyo Research; the Osaka Foundation for the Promotion of Clinical Immunology; and the Takeda Science Foundation.

1. Bouma G, Strober W (2003) The immunological and genetic basis of inflammatory bowel disease. *Nat Rev Immunol* 3:521–533.
2. Xavier RJ, Podolsky DK (2007) Unravelling the pathogenesis of inflammatory bowel disease. *Nature* 448:427–434.
3. Strober W, Fuss I, Mannon P (2007) The fundamental basis of inflammatory bowel disease. *J Clin Invest* 117:514–521.
4. Wing K, Sakaguchi S (2010) Regulatory T cells exert checks and balances on self tolerance and autoimmunity. *Nat Immunol* 11:7–13.
5. Sakaguchi S, Wing K, Onishi Y, Prieto-Martin P, Yamaguchi T (2009) Regulatory T cells: How do they suppress immune responses? *Int Immunol* 21:1105–1111.
6. Morelli AE, Thomson AW (2007) Tolerogenic dendritic cells and the quest for transplant tolerance. *Nat Rev Immunol* 7:610–621.
7. Wakkach A, et al. (2003) Characterization of dendritic cells that induce tolerance and T regulatory 1 cell differentiation in vivo. *Immunity* 18:605–617.
8. Gabrilovich DI, Nagaraj S (2009) Myeloid-derived suppressor cells as regulators of the immune system. *Nat Rev Immunol* 9:162–174.
9. Ostrand-Rosenberg S, Sinha P (2009) Myeloid-derived suppressor cells: Linking inflammation and cancer. *J Immunol* 182:4499–4506.
10. Laffont S, Powrie F (2009) Immunology: Dendritic-cell genealogy. *Nature* 462: 732–733.
11. Strober W (2009) The multifaceted influence of the mucosal microflora on mucosal dendritic cell responses. *Immunity* 31:377–388.
12. Coombes JL, Powrie F (2008) Dendritic cells in intestinal immune regulation. *Nat Rev Immunol* 8:435–446.
13. Varol C, et al. (2009) Intestinal lamina propria dendritic cell subsets have different origin and functions. *Immunity* 31:502–512.
14. Bogunovic M, et al. (2009) Origin of the lamina propria dendritic cell network. *Immunity* 31:513–525.
15. Niess JH, Adler G (2010) Enteric flora expands gut lamina propria CX3CR1+ dendritic cells supporting inflammatory immune responses under normal and inflammatory conditions. *J Immunol* 184:2026–2037.
16. Johansson-Lindbom B, et al. (2005) Functional specialization of gut CD103+ dendritic cells in the regulation of tissue-selective T cell homing. *J Exp Med* 202:1063–1073.
17. Schulz O, et al. (2009) Intestinal CD103+, but not CX3CR1+, antigen sampling cells migrate in lymph and serve classical dendritic cell functions. *J Exp Med* 206: 3101–3114.
18. Coombes JL, et al. (2007) A functionally specialized population of mucosal CD103+ DCs induces Foxp3+ regulatory T cells via a TGF-beta and retinoic acid-dependent mechanism. *J Exp Med* 204:1757–1764.
19. Sun CM, et al. (2007) Small intestine lamina propria dendritic cells promote de novo generation of Foxp3 T reg cells via retinoic acid. *J Exp Med* 204:1775–1785.
20. Matteoli G, et al. (2010) Gut CD103+ dendritic cells express indoleamine 2,3-dioxygenase which influences T regulatory/T effector cell balance and oral tolerance induction. *Gut* 59:595–604.
21. Uematsu S, et al. (2008) Regulation of humoral and cellular gut immunity by lamina propria dendritic cells expressing Toll-like receptor 5. *Nat Immunol* 9:769–776.
22. Denning TL, Wang YC, Patel SR, Williams IR, Pulendran B (2007) Lamina propria macrophages and dendritic cells differentially induce regulatory and interleukin 17-producing T cell responses. *Nat Immunol* 8:1086–1094.
23. Atarashi K, et al. (2008) ATP drives lamina propria T(H)17 cell differentiation. *Nature* 455:808–812.
24. Manocha M, et al. (2009) Blocking CD27-CD70 costimulatory pathway suppresses experimental colitis. *J Immunol* 183:270–276.
25. Ueda Y, et al. (2010) Commensal microbiota induce LPS hyporesponsiveness in colonic macrophages via the production of IL-10. *Int Immunol* 22:953–962.
26. Murai M, et al. (2009) Interleukin 10 acts on regulatory T cells to maintain expression of the transcription factor Foxp3 and suppressive function in mice with colitis. *Nat Immunol* 10:1178–1184.
27. Manicassamy S, et al. (2010) Activation of beta-catenin in dendritic cells regulates immunity versus tolerance in the intestine. *Science* 329:849–853.
28. Siddiqui KR, Laffont S, Powrie F (2010) E-cadherin marks a subset of inflammatory dendritic cells that promote T cell-mediated colitis. *Immunity* 32:557–567.
29. Takada Y, et al. (2010) Monocyte chemoattractant protein-1 contributes to gut homeostasis and intestinal inflammation by composition of IL-10-producing regulatory macrophage subset. *J Immunol* 184:2671–2676.
30. Jung S (2010) Dendritic cells: A question of upbringing. *Immunity* 32:502–504.
31. Kühn R, Löhler J, Rennick D, Rajewsky K, Müller W (1993) Interleukin-10-deficient mice develop chronic enterocolitis. *Cell* 75:263–274.
32. Takeda K, et al. (1999) Enhanced Th1 activity and development of chronic enterocolitis in mice devoid of Stat3 in macrophages and neutrophils. *Immunity* 10:39–49.
33. Kobayashi M, et al. (2003) Toll-like receptor-dependent production of IL-12p40 causes chronic enterocolitis in myeloid cell-specific Stat3-deficient mice. *J Clin Invest* 111: 1297–1308.
34. Melillo JA, et al. (2010) Dendritic cell (DC)-specific targeting reveals Stat3 as a negative regulator of DC function. *J Immunol* 184:2638–2645.
35. Niess JH (2010) What are CX3CR1+ mononuclear cells in the intestinal mucosa? *Gut Microbes* 1:396–400.
36. Scott CL, Aumeunier AM, Mowat AM (2011) Intestinal CD103+ dendritic cells: Master regulators of tolerance? *Trends Immunol* 32:412–419.
37. Medina-Contreras O, et al. (2011) CX3CR1 regulates intestinal macrophage homeostasis, bacterial translocation, and colitogenic Th17 responses in mice. *J Clin Invest* 121:4787–4795.
38. Youn JI, Nagaraj S, Collazo M, Gabrilovich DI (2008) Subsets of myeloid-derived suppressor cells in tumor-bearing mice. *J Immunol* 181:5791–5802.
39. Iliev ID, Mileti E, Matteoli G, Chieppa M, Rescigno M (2009) Intestinal epithelial cells promote colitis-protective regulatory T-cell differentiation through dendritic cell conditioning. *Mucosal Immunol* 2:340–350.
40. Iliev ID, et al. (2009) Human intestinal epithelial cells promote the differentiation of tolerogenic dendritic cells. *Gut* 58:1481–1489.
41. Ishii M, et al. (2009) Sphingosine-1-phosphate mobilizes osteoclast precursors and regulates bone homeostasis. *Nature* 458:524–528.
42. Jung S, et al. (2000) Analysis of fractalkine receptor CX(3)CR1 function by targeted deletion and green fluorescent protein reporter gene insertion. *Mol Cell Biol* 20: 4106–4114.

DOI/10.1007/s10059-011-1010-x

Minireview

Molecules and Cells

The Role of Sphingosine 1-Phosphate in Migration of Osteoclast Precursors; an Application of Intravital Two-Photon Microscopy

Taeko Ishii, Yutaka Shimazu, Issei Nishiyama, Junichi Kikuta, and Masaru Ishii*

Sphingosine-1-phosphate (S1P), a biologically active lysophospholipid that is enriched in blood, controls the trafficking of osteoclast precursors between the circulation and bone marrow cavities via G protein-coupled receptors, S1PRs. While S1PR1 mediates chemoattraction toward S1P in bone marrow, where S1P concentration is low, S1PR2 mediates chemorepulsion in blood, where the S1P concentration is high. The regulation of precursor recruitment may represent a novel therapeutic strategy for controlling osteoclast-dependent bone remodeling. Through intravital multiphoton imaging of bone tissues, we reveal that the bidirectional function of S1P temporospatially regulates the migration of osteoclast precursors within intact bone tissues. Imaging technologies have enabled *in situ* visualization of the behaviors of several players in intact tissues. In addition, intravital microscopy has the potential to be more widely applied to functional analysis and intervention.

INTRODUCTION

Bone is a highly dynamic organ that is continuously turned over during growth, even in adults. During bone remodeling, homeostasis is regulated by the balance between bone formation by osteoblasts and bone resorption by osteoclasts (Harada et al., 2003; Teitelbaum et al., 2003). However, in pathological conditions such as osteoporosis, osteopetrosis, arthritic joint destruction, and bone metastasis, this equilibrium is disrupted. Since osteoclasts are excessively activated in osteolytic diseases, the inhibition of osteoclast function has been a major therapeutic strategy. Bisphosphonates, the most widely used group of anti-osteoporosis drugs, bind to hydroxyapatite, enter osteoclasts via endocytosis, and induce osteoclast apoptosis (Russell et al., 2007). Recently, the inactivation of osteoclasts, as opposed to their elimination, has generated interest as an alternative treatment strategy (Deal, 2009; Yasuda et al., 2005). One promising regulation point is the recruitment of osteoclast precursors. In addition to several chemokines that are known regulators of migration, including CXCL12 (Yu et al., 2003) and CX_3CL1 (Koizumi et al., 2009), we have shown that sphingosine 1-phosphate (S1P), a lysophospholipid abundant in the plasma, plays an important role as both a chemoattractant and a chemorepellent (Ishii et al., 2009; 2010). In this review, we summarize the bidirectional regulation of osteoclast precursor migration by S1P and briefly describe intravital bone imaging in living animals.

S1P and its receptors

S1P is a bioactive sphingolipid metabolite that regulates diverse biological functions including cell proliferation, motility, and survival (Cyster, 2005; Rivera et al., 2008; Rosen et al., 2005; 2007). Sphingolipids are essential plasma membrane constituents composed of a serine head group and one or two fatty acid tails. They are easily metabolized and converted to sphingosines, which are ATP-dependently phosphorylated by sphingosine kinases 1 and 2 (SPHK1 and SPHK2) in most cells, yielding S1P (Hannun et al., 2008). SPHKs, which are regulated by a variety of growth factors, hormones, and cytokines, control S1P's acute reactive generation and homeostasis in the circulation (Hannun et al., 2008). Immediately after its synthesis, free S1P is irreversibly degraded by intracellular S1P lyase or dephosphorylated by S1P phosphatases. As a result, the levels of S1P in most tissues, including bone marrow, are relatively low. In contrast, large amounts of S1P are continuously produced in the plasma, especially by erythrocytes, and the serum concentration of S1P is extremely high (several hundred nanomolar to low-micromolar range). Most S1P in the circulation is bound to high-density lipoprotein (HDL) and albumin, which serve as stable reservoirs and efficiently deliver S1P to epithelial cell-surface receptors (Argraves et al., 2008). In addition, because S1P is an amphiphilic molecule that cannot easily cross membranes, an S1P gradient between the blood and tissues is maintained.

S1P signals via five 7-transmembrane receptors or G protein-coupled receptors (GPCRs), S1PR1 to S1PR5, previously referred to as endothelial differentiation gene (Edg) receptors (Rivera et al., 2008; Rosen et al., 2007). Because of the different distribution of these receptors and their different coupling to signal-transducing G proteins, S1P shows a broad range of

Laboratory of Biological Imaging, WPI-Immunology Frontier Research Center, Osaka University, Osaka, Japan
*Correspondence: mishii@ifrec.osaka-u.ac.jp

Received January 13, 2011; accepted January 31, 2011; published online February 25, 2011

Keywords: cell dynamics, chemokine, chemotaxis, lipid mediator, live imaging

Table 1. S1P receptors and phenotypes of their genetic deletion

S1P Receptors	S1PR1	S1PR2	S1PR3	S1PR4	S1PR5
Coupling G proteins	$G_{i/O}$	G_i G_q G_s $G_{12/13}$	G_i G_q G_s $G_{12/13}$	G_i $G_{12/13}$	$G_{i/o}$ $G_{12/13}$
Distribution	Ubiquitous	Ubiquitous Highest expressed in embryonic brain Expressed high in adult heart and lung	Spleen, heart, lung, thymus, kidney, testis, brain, skeletal muscle	Thymus, spleen, lung, peripheral leukocytes	Brain, spleen, peripheral leukocytes
Phenotypes of gene deletion (mouse)	Embryonic lethal (e12.5-e14.5)	Vestibular defects Hearing loss Seizures (C57BL/6 only) Perinatal lethal (reduce litter size) Survivours show no phonotype	Disruption of alveolar epithelial junctions	Ddisorder of mega-karyocyte differentiation	Reduced number of NK cells
Biological function	Rac activation	Rho activation Vasoconstriction angiogenesis Wound healing	Cardioprotection by HDL		
References	Liu et al. (2000) Matloubian et al. (2004)	Kono et al. (2007) Serriere-Lanneau et al. (2007)	Nofer et al. (2004) Gon et al. (2005)	Golfier et al. (2010)	Walzer et al. (2007)

Cyster et al. (2005), Rivera et al. (2008), Rosen et al. (2005; 2007).

bioactivities (Table 1). S1PR1 is ubiquitously expressed and primarily coupled to PTX-sensitive $G_{i/o}$ proteins, whereas S1PR2 and S1PR3, whose distributions are more limited, are coupled to $G_{12/13}$ as well as G_q, G_s, and G_i. The expression of S1PR4 and S1PR5 is much lower than that of S1PR1, S1PR2, and S1PR3, and their functions remain to be elucidated. However, it has been reported that they are coupled to $G_{i/o}$ and $G_{12/13}$.

S1P receptors have key roles in the regulation of cellular motility. S1PR1 activates Rac through Gi and promotes cell migration and intercellular connection, whereas S1PR2 activates Rho signaling via $G_{12/13}$, thereby counteracting the effects of S1PR1 and inhibiting Rac activity (Takuwa, 2002). These differences account for the different biological functions of S1PR1 and S1PR2, which produce opposite effects on migration toward/against S1P gradients *in vitro* (Okamoto et al., 2000).

Osteoclast precursors and S1P

Osteoclasts are derived from macrophage/monocyte-lineage cells that express both S1PR1 and S1PR2 (Ishii et al., 2009). As described above, S1PR1 and S1PR2 have opposite effects on the migration of osteoclast precursors. Osteoclast precursors are chemoattracted to S1P *in vitro*, a response that is blocked by PTX. In addition, treatment with S1P increases osteoclast precursor levels of the active form of Rac (GTP-Rac), suggesting that Rac and Gi are involved in S1PR1 chemotactic signaling in osteoclast precursors. On the other hand, S1PR2 requires a higher concentration of S1P for activation and induces negative chemotactic responses, "chemorepulsion," to S1P gradients. S1PR2 activation causes cells to move from the bloodstream into bone marrow cavities (Ishii et al., 2010). As in leukocytes, the migration of osteoclast precursors is regulated by chemokines. Like the S1PRs, chemokine receptors are GPCRs and signal via Gi components. One of the best-known chemoattractants for osteoclast precursors is CXCL12 (also known as stromal derived factor-1), a CXCR4 ligand (Yu et al., 2003). CXCL12 is constitutively expressed at high levels by osteoblastic stromal cells and vascular endothelial cells in bone, whereas CXCR4 is expressed on a wide variety of cells types, including circulating monocytes and osteoclast precursors. CXCL12 has chemotactic effects on osteoclast precursors, which express large amounts of CXCR4.

Recently, another chemokine, CX_3CL1 (also known as fractalkine), which functions as a membrane-bound adhesion molecule, was shown to act as a chemoattractant after its cleavage by ADAM10 and ADM7. Expressed by osteoblastic stromal cells, it was reported to be involved in both the recruitment and attachment of osteoclast precursors (Koizumi et al., 2009). Expression of both chemokine receptors and S1PRs is reduced by RANKL stimulation, dependent on NF-κB, but not on NF-AT. Presumably, after cells mature and arrive at their ultimate destinations these chemoattractants are no longer needed.

Application of intravital imaging to the analysis of cell behavior in bone

To study the behavior of osteoclasts and their precursors *in vivo*, we developed a new intravital two-photon imaging system for use in the analysis of bone tissues (Fig. 1) (Ishii et al., 2009; 2010). Recent advances in microscope, laser, and fluorophore technology have made it possible to visualize living cells in intact organs and to analyze their mobility and interactions in a quantitative manner.

As calcium phosphate, the main structural component of the bone matrix, can scatter laser beams, it was difficult to access the deep interior of bone tissues, even using a near-infrared laser. We decided to use parietal bone in which the distance from the bone surface to the bone marrow cavity is 80-120 μm (within the appropriate range for two-photon microscopy). We

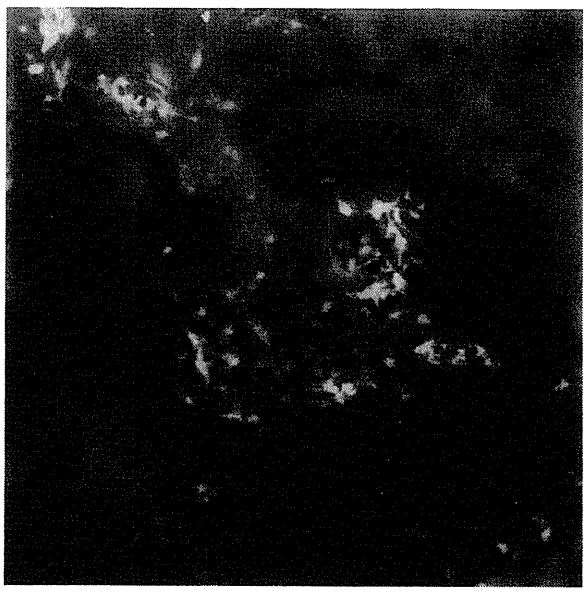

Fig. 1. Bone marrow structure visualized by intravital two-photon imaging. Murine skull bone tissues of heterozygous Cx_3CR1-EGFP knock-in mice. Collagen fibers in bone are detected by second-harmonic generation (in blue), and the microvasculature are visualized by intravenous injection of 70 kDa dextran-conjugated Texas Red. CX_3CR1-EGFP positive cells appear green in bone marrow cavity.

modified the method used in a pilot study, which revealed that central memory $CD8^+$ T cells were preferentially recruited to, and accumulated in, the bone marrow cavity and interacted with mature circulating dendritic cells (Cavanagh et al., 2005; Mazo et al., 2005).

Using this new intravital two-photon imaging method, we showed that S1P controls the migratory behavior of osteoclast precursors, dynamically regulating bone mineral homeostasis, and we identified a critical control point in osteoclastogenesis. While monocytoid cells containing osteoclast precursors (CSF1R-EGFP-positive or CX3CR1-EGFP-positive cells) were stationary at the steady state, osteoclast precursors were stimulated and moved into vessels when a potent S1PR1-specific agonist, SEW2871 (Wei et al., 2005), was injected intravenously.

To clarify the physiological significance of S1P-directed chemotaxis of osteoclast precursors in bone homeostasis, we examined osteoclast/monocyte-specific S1PR1-deficient ($S1PR1^{-/-}$) mice. [Global S1PR1 deficiency causes embryonic lethally at e12.5 to e14.5 due to defective blood vessel development (Liu et al., 2000)]. The attachment of osteoclast precursors to bone surfaces was significantly enhanced in $S1PR1^{-/-}$ animals compared with controls. $S1PR1^{-/-}$ osteoclasts precursors on bone surfaces subsequently develop into mature osteoclasts and absorb bone tissues. S1P-mediated chemotaxis of osteoclast precursors would thus be expected to contribute to their redistribution from bone tissues to blood vessels.

We also performed intravital two-photon imaging of bone tissues to define the role of S1PR2 *in vivo* (Ishii et al., 2010). We showed that certain osteoclast precursors (CX_3CR1-EGFP-positive cells) moved into the bloodstream when a potent S1PR2 antagonist, JTE013 (Osada et al., 2002), was injected intravenously. The effect of JTE013 was less pronounced than that of the S1PR1 agonist SEW2871. Furthermore, to clarify the physiological significance of $S1P^{-/-}$ chemotaxis of osteoclast precursors in bone homeostasis, we examined S1PR2-deficient ($S1PR2^{-/-}$) mice. Although $S1PR2^{-/-}$ mice suffer auditory impairment due to vessel defects in the inner ear, they survive and reproduce (Kono et al., 2007). Although bone resorption of osteoclasts was significantly lower in $S1PR2^{-/-}$ animals than in controls, *in vitro* osteoclast formation was not significantly affected. In a high-S1P environment such as the bloodstream, S1PR1 is activated and rapidly internalized, allowing S1PR2 to predominate. Osteoclast precursors enter the bone marrow as a result of chemorepulsion mediated by S1PR2, and other chemo-

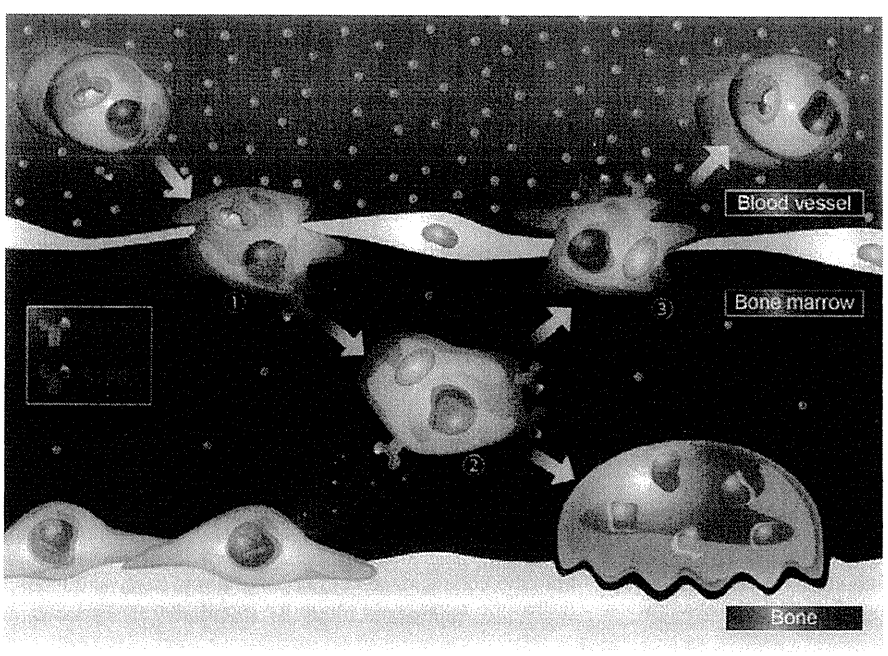

Fig. 2. A schematic model for S1P-mediated osteoclast precursors localization. The entry of osteoclast precursors from blood vessels where S1P is at high concentration, is initiated by chemorepulsion through S1PR2 (1). Once enter in bone marrow, osteoclast precursors migrate toward chemokines enriched in bone marrow cavity (2). On the other hand, their recirculation toward blood vessels is regulated by chemoattraction through S1PR1 (3).

kines attract them to bone surfaces. After they enter a low-S1P environment such as bone marrow, S1PR1 is transported back to the cell surface, and osteoclast precursors return from bone tissues to blood vessels as a result of chemotaxis to an S1P gradient.

The number of osteoclast precursors on bone surfaces is determined by the balance between the trafficking of osteoclast precursors to and from the circulation. These data provide evidence that S1P controls the migratory behavior of osteoclast precursors, dynamically regulating bone mineral homeostasis, and identify a critical control point in osteoclastogenesis. Based on our findings, we propose that regulation of the migratory behavior of osteoclast precursors controls osteoclast differentiation. This control mechanism is summarized in Fig. 2. This critical control point in osteoclastogenesis may represent an attractive target for new treatments for osteoporosis. We previously showed that treatment with FTY720, which is metabolized by SPHK2 to a compound that acts as an agonist for four of the five S1P receptors (not S1PR2) (Cyster, 2005; Matloubian et al., 2004), relieved ovariectomy-induced osteoporosis in mice by reducing the number of mature osteoclasts attached to bone surfaces (Ishii et al., 2009). The mechanism of action of S1P is completely different from that of conventional treatments such as bisphosphonates, which suppress mature osteoclasts. We anticipate that the regulation of osteoclast precursor migration may be a useful clinical strategy in the near future.

FTY720 is a reversible immunosuppressive agent approved as a treatment for multiple sclerosis in the United States. It induces lymphopenia by confining lymphocytes to lymphoid organs (Mandala et al., 2002). The precise mechanisms behind this phenomenon remain controversial, and it is necessary to determine how FTY720 produces the opposite effect on monocyte-macrophage cells in bone marrow (which are expelled into the circulation by FTY720).

Future directions for two-photon microscopy

Two-photon intravital imaging has revealed, and continues to reveal, dynamic features of physiological and pathological process. Its greatest strength is its ability to provide spatiotemporal information in living organisms, which cannot be achieved using other methods. However, current two-photon microscopy imaging techniques have several limitations. First, we cannot see everything in the visual fields in two-photon microscopy. Although fluorescence labeling and second-harmonic generation enable us to observe target cells and organs, the lack of a signal does never reflect an open field, as diverse structures and cellular components should be present. To avoid misinterpretation, we must interpret our observations with caution. Second, although two-photon microscopy has greater penetration depth than conventional confocal microscopy, its penetration depth is only 800-1000 μm in soft tissues (e.g., brain cortex) and 200 μm in hard tissues (e.g., bone). Because of these resolution limitations, it may only be applied to small animals, such as mice and rats. Moreover, due to the wide scattering of light by the skin, it is necessary that target organs should be exteriorized. It is possible that the necessary operative invasion and changes in oxygen concentration and humidity may influence cellular behavior. To resolve these problems, technical innovations in fluorochrome and optical systems, including improvements in light emission and amelioration of resolution problems (Ntziachristos, 2010), are needed.

Intravital microscopy has begun to be applied not only to observational studies, but also to functional analysis and interventions. Recently, several new fluorescence tools have been developed. These include cell-cycle indicators (Sakaue-Sawano et al., 2008) and light-sensing devices such as photoactivatable fluorescent proteins (Victora et al., 2010) and light-induced activators of G protein-coupled receptors (Airan et al., 2009).

CONCLUSION

As the recruitment of osteoclast precursors during osteoclastogenesis is dynamic and dependent on the microenvironment of the bone marrow cavity, temporospatial information is very important. Intravital imaging has made a huge contribution to improving our understanding of these processes. It enables us to visualize, temporospatially, complicated systems in living organisms. This new technique has revealed that S1P acts in concert with several chemoattractants to shepherd osteoclast precursors to appropriate sites. Controlling the recruitment and migration of osteoclast precursors represents a promising new therapeutic strategy for combating bone diseases. Although their limitations remain to be resolved, the range of applications for *in vivo* imaging techniques continues to expand.

REFERENCES

Airan, R.D., Thompson, K.R., Fenno, L.E., Bernstein, H., and Deisseroth, K. (2009). Temporally precise *in vivo* control of intracellular signalling. Nature *458*, 1025-1029.

Argraves, K.M., Gazzolo, P.J., Groh, E.M., Wilkerson, B.A., Matsuura, B.S., Twai, W.O., Hammad, S.M., and Argraves, W.S. (2008). High density lipoprotein-associated sphingosine 1-phosphate promotes endothelial barrier function. J. Biol. Chem. *283*, 25074-25081.

Cavanagh, L.L., Bonasio, R., Mazo, I.B., Halin, C., Cheng, G., van der Velden, A.W., Cariappa, A., Chase, C., Russell, P., Starnbach, M.N., et al. (2005). Activation of bone marrow-resident memory T cells by circulating antigen-bearing dendritic cells. Nat. Immunol. *6*, 1029-1037.

Cyster, J.G. (2005). Chemokines, sphingosine-1-phosphate, and cell migration in secondary lymphoid organs. Annu. Rev. Immunol. *23*, 127-159.

Deal, C. (2009). Future therapeutic targets in osteoporosis. Curr. Opin. Rheumatol. *4*, 380-385.

Golfier, S., Kondo, S., Schulze, T., Takeuchi, T., Vassileva, G., Achtman, A.H., Gräler, M.H., Abbondanzo, S.J., Wiekowski, M., Kremmer, E., et al. (2010). Shaping of terminal megakaryocyte differentiation and proplatelet development by sphingosine-1-phosphate receptor S1P4. FASEB J. *24*, 4701-4710.

Gon, Y., Wood, M.R., Kiosses, W.B., Jo, E., Sanna, M.G., Chun, J., and Rosen, H. (2005). S1P3 receptro-induced reorganization of epithelial tight junctions compromises lung barrier integritiy and is potentiated by TNF. Proc. Natl. Acad. Sci. USA *102*, 9270-9275.

Hannun, Y.A., and Obeid, L.M. (2008). Principles of bioactive lipid signaling: lessons from sphingolipids. Nat. Rev. Mol. Cell. Biol. *9*, 139-150.

Harada, S., and Rodan, G.A. (2003). Control of osteoblast function and regulation of bone mass. Nature *423*, 349-355.

Ishii, M., Egen, J.G., Klauschen, F., Meier-Schellersheim, M., Saeki, Y., Vacher, J., Proia, R.L., and Germain, R.N. (2009). Sphingosine-1-phosphate mobilizes osteoclast precursors and regulates bone homeostasis. Nature *458*, 524-528.

Ishii, M., Kikuta, J., Shimazu, Y., Meier-Schellersheim, M., and Germain, R.N. (2010). Chemorepulsion by blood S1P regulates osteoclast precursor mobilization and bone remodeling *in vivo*. J. Exp. Med. *207*, 2793-2798.

Koizumi, M., Saitoh, Y., Minami, T., Takeno, N., Tsuneyama, K., Miyahara, T., Nakayama, T., Sakurai, H., Takano, Y., Nishimura, M., et al. (2009). Role of CX3CL1/fractalkine in osteoclast differentiation and bone resorption. J. Immunol. *183*, 7825-7831.

Kono, M., Belyantseva, I.A., Skoura, A., Frolenkov, G.I., Starost, M.F., Dreier, J.L., Lidngton, D., Bolz, S.S., Friedman, T.B., Hla, T., et al. (2007). Deafness and stria vascularis defects in S1P2 receptor-null mice. J. Biol. Chem. *282*, 10690-10696.

Liu, Y., Wada, R., Yamashita, T., Mi, Y., Deng, C.X., Hobson, J.P., Rosenfeldt, H.M., Nava, V.E., Chae, S.S., Lee, M.J., et al.

(2000). Edg-1, the G-protein-coupled receptor for sphingosine-1-phosphate, is essential for vascular maturation. J. Clin. Invest. *106*, 951-961.

Mandala, S., Hajdu, R., Bergstrom, J., Quackenbush, E., Xie, J., Milligan, J., Thornton, R., Shei, G.J., Card, D., Keohane, C., et al. (2002). Alteration of lymphocyte trafficking by sphingosine-1-phosphate receptor agonists. Science *296*, 346-349.

Matloubian, M., Lo, C.G., Cinamon, G., Lesneski, M.J., Xu, Y., Brinkmann, V., Allende, M.L., Proia, R.L., and Cyster, J.G. (2004). Lymphocyte egress from thymus and peripheral lymphoid organs is dependent on S1P receptor 1. Nature *6972*, 355-360.

Mazo, I.B., Honczarenko, M., Leung, H., Cavanagh, L.L., Bonaisio, R., Weninger, W., Engelke, K., Xia, L., McEver, R.P., Koni, P.A., et al. (2005). Bone marrow is a major reservoir and site of recruitment for central memory CD8+ T cells. Immunity *22*, 259-270.

Nofer, J.R., van der Giet, M., Tolle, M., Wolinska, I., von Wnuck Lipinski, K., Baba, H.A., Tietge, U.J., Godecke, A., Ishii, I., Kleuser, B., et al. (2004). HDL induces NO-dependent vasorelaxation via the lysophospholipid receptor S1P3. J. Clin. Invest. *113*, 569-581.

Ntziachristos, V. (2010). Going deeper than microscopy: the optical imaging frontier in biology. Nat. Methods *7*, 603-614.

Okamoto, H., Takuwa, N., Yokomizo, T., Sugimoto, N., Sakurada, S., Shigematsu, H., and Takuwa, Y. (2000). Inhibitory regulation of Rac activation, membrane ruffling, and cell migration by the G protein-coupled sphingosine-1-phosphate receptor EDG5 but not EDG1 or EDG3. Mol. Cell. Biol. *20*, 9247-9261.

Osada, M., Yatomi, Y., Ohmori, T., Ikeda, H., and Ozaki, Y. (2002). Enhancement of sphingosine 1-phosphate-induced migration of vascular endothelial cells and smooth muscle cells by an EDG-5 antagonist. Biochem. Biophys. Res. Commun. *299*, 483-487.

Rivera, J., Proia, R.L., and Olivera, A. (2008). The alliance of sphingosine-1-phosphate and its receptors in immunity. Nat. Rev. Immunol. *8*, 753-763.

Rosen, H., and Goetzl, E.J. (2005). Sphingosine 1-phosphate and its receptors: an autocrine and paracrine network. Nat. Rev. Immunol. *5*, 560-570.

Rosen, H., Sanna, M.G., Cahalan, S.M., and Gonzalez-Cabrera, P.J. (2007). Tipping the gatekeeper: S1P regulation of endothelial barrier function. Trends Immunol. *28*, 102-107.

Russell, R.G.G., Xia, Z., Dunford, J.E., Oppermann, U., Kwaasi, A., Hulley, P.A., Kavanagh, K.L., Triffitt, J.T., Lundy, M.W., Phipps, R.J., et al. (2007). Bisphosphonates. An update on mechanisms of action and how these relate to clinical efiicacy. Ann. N Y Acad. Sci. *1117*, 209-257.

Sakaue-Sawano, A., Kurokawa, H., Morimura, T., Hanyu, A., Hama, H., Osawa, H., Kashiwagi, S., Fukami, K, Miyata, T., Miyoshi, H., et al. (2008). Visualizing spatiotemporal dynamics of multicellular cell-cycle progression. Cell *132*, 487-498.

Serrier-Lanneau, V., Teixeira-Clerc, F., Li, L., Schippers, M., de Wris, W., Julien, B., Tran-Van-Nhieu, J., Manin, S., Pelstra, K., Chun J., et al. (2007). The sphingosine 1-phosphate receptor S1P2 triggers hepatic wound healing. FASEB J. *21*, 2005-2013.

Takuwa, Y. (2002). Subtype-specific differential regulation of Rho family G proteins and cell migration by the Edg family sphingosine-1-phosphate receptors. Biochem. Biophys. Acta *1682*, 112-120.

Teitelbaum, S.L., Ross, F.P. (2003). Genetic regulation of osteoclast development and function. Nat. Rev. Genetic. *4*, 638-649

Victora, G.D., Schwichkert, T.A., Fooksman, D.R., Kamphorst, A.O., Meyer-Hermann, M., Dustin, M.L., and Nussenzweig, M.C. (2010). Germinal center dynamics revealed by multiphoton microscopy with a photoactivatable fluorescent reporter. Cell *143*, 592-605

Wei, S.H., Rosen, H., Matheu, M.P., Sanna, M.G., Wang, S.K., Jo, E., Wong, C.H., Parker, I., and Cahalan, M.D. (2005). Sphingosine 1-phospate type 1 receptor agonism inhibits transendothelial migration of medullary T cells to lymphatic sinuses. Nat. Immunol. *12*, 1228-1235.

Yasuda, Y., Kaleta, J., and Bromme, D. (2005). The role of cathepsins in osteoporosis and arthritis: rationale for the design of new therapeutics. Adv. Drug. Deliv. Rev. *57*, 973-993.

Yu, X., Huang, Y., Collin-Osdoby, P., and Osdoby, P. (2003). Stromal cell-derived factor-1 (SDF-1) recruits osteoclast precursors by inducing chemotaxis, matrix metalloproteinase-9 (MMP-9) acrivity, and collagen transmigration. J. Bone Miner. Res. *18*, 1404-1418.

SUPPLEMENT

How do contemporary imaging techniques contribute to basic and clinical rheumatology?

Masaru Ishii[1,2]

[1]Laboratory of Cellular Dynamics, WPI-Immunology Frontier Research Center, Osaka University, Osaka, Japan
[2]Japan Science and Technology Agency, CREST

Correspondence to
Masaru Ishii, Laboratory of Cellular Dynamics, WPI-Immunology Frontier Research Center, Osaka University, 3-1 Yamada-oka, Suita, Osaka 565-0871, Japan;
mishii@ifrec.osaka-u.ac.jp

Received 10 August 2011
Accepted 25 September 2011

ABSTRACT

Recent major advances in biomedical imaging techniques have allowed us to visualise a variety of previously unseen biological phenomena. In particular, advanced fluorescent microscopy and radioimaging have enabled us to visualise cellular and molecular dynamics in living animals and humans. These new technologies have identified novel therapeutic targets against a wide array of diseases and have provided novel diagnostic tools for the evaluation of several disease conditions. In this brief review, the author outlines the contemporary imaging techniques used in the fields of immunology and rheumatology, with special focus on intravital fluorescent microscopy, and discusses how these cutting-edge methodologies contribute to clinical practice for patients with rheumatism.

Immune systems are highly dynamic, and the proper migration and localisation of relevant cell types are critically important for the maintenance of immune reactions. Classical analyses such as histological sectioning provide merely a snapshot of cellular localisation and molecular distribution but cannot provide temporal information. Recent advances in biological imaging techniques have revolutionised the biomedical sciences, and researchers can now obtain spatiotemporal information about the immune and inflammatory systems.

Here, the recently developed cutting-edge technology in optical microscopic imaging systems for the detection of cellular dynamics in intact tissues and organs, such as intravital multiphoton microscopy, is briefly introduced, and the findings closely related to the fields of rheumatology and immunology that could be discovered by this novel methodology are discussed. The possible use of radioimaging techniques for the evaluation of human immune systems is also described. Based on these technical advancements, the ways in which this new trend in biomedical sciences could contribute to the development of a new era in clinical rheumatology is discussed.

Intravital multiphoton imaging: a revolutionary tool for immunological studies

Recent advances in fluorescent microscopic techniques have revolutionised biological sciences; among them, the development and improved usability of two-photon excitation microscopy have enabled us to visualise biological phenomena that cannot be seen with conventional methods, such as the dynamic behaviour of cells deep inside living organs. In conventional fluorescent microscopy, a fluorophore absorbs energy from a single photon and then releases the energy as an emission photon. In multiphoton (normally two-photon) excitation mode, a fluorophore absorbs multiple photons simultaneously. This non-linear optical process can occur only in areas with extremely high photon density, such as the focal plane of optical paths. The limited excitation enables us to acquire bright and high-resolution images in regions deep inside tissues and organs. Near-infrared lasers used for multiphoton excitation can penetrate deeper, with less absorption or scattering, than the visible light used with confocal microscopy. Thus, objects can be visualised at depths of 100–1000 μm with two-photon excitation (table 1), whereas conventional imaging modalities such as confocal microscopy can only access areas at depths of less than 100 μm.[1] This property is beneficial for the analysis of live biological systems. The cells observed in a fixed and thin-sectioned sample are dead and no longer moving. The intravital visualisation of live dynamic systems often requires the observation of areas deep below the surface, which can only be achieved by two-photon excitation microscopy. Moreover, multiphoton excitation with near-infrared light can minimise photo bleaching and phototoxicity, thereby reducing damage to the imaged tissues and organs.[2 3]

Intravital multiphoton imaging has revolutionised biological research, especially in the field of immunology, where the cells comprising various immune tissues and organs are dynamic. For example, dynamic observations in lymph nodes have revealed the migratory changes in T cells in close contact with antigen-presenting dendritic cells.[4–6] When T cells encounter antigen-bearing dendritic cells, they form stable contacts lasting for at least several hours for priming and thereafter regain motility for recirculation. In thymic organ cultures, intravital imaging has shown interactions between thymocytes and stromal cells during positive and negative selection.[7] Live imaging has been tested for the visualisation of immune cell inflammatory reactions in many other tissues, such as those in the skin,[8] the lungs,[9] the liver[10] and the small intestine,[11] and has revealed various critical biological phenomena in each system.

The bone is a mineralised hard tissue that limits the passage of visible or infrared lasers, and it has long been considered to be extremely difficult to observe intact bone tissues in living animals.[12] We have developed a novel imaging system for visualisation inside bone cavities with high spatiotemporal resolution (figure 1). By using this technique, we can demonstrate that osteoclasts and their precursors migrate and localise under the control of several chemokines

Table 1 Comparison of optical imaging and radioimaging for studying medical sciences

	Optical imaging (multiphoton microscopy)	Radioimaging (positron emission tomography)
Spatial resolution	High (~1–10 μm)	Low (~1–10 mm)
Temporal resolution	High (0.1–10 s)	Low (10–30 min)
Visual field	Narrow (100–1000 μm)	Wide (100–2000 mm)
Depth of imaged areas	Shallow (100–1000 μm)	Deep (~1000 mm)
Multi-colour labelling	Possible	Impossible
Possible application for clinical rheumatology	- Revealing rapid cellular dynamics at local sites of inflammation (migratory behaviour, cell–cell interaction, etc)	- Revealing subacute/chronic changes of inflammation in total body (accumulation of immune cells and inflammatory molecules, etc)
	- Can only visualise the areas adjacent to the surface (eg, skin inflammation)	- Can visualise the events occurring deep inside the body
	- But can detect deeper areas with endoscope approaches (eg, gastrointestinal tracts, abdomen and joints)	- Spatiotemporal resolution is limited

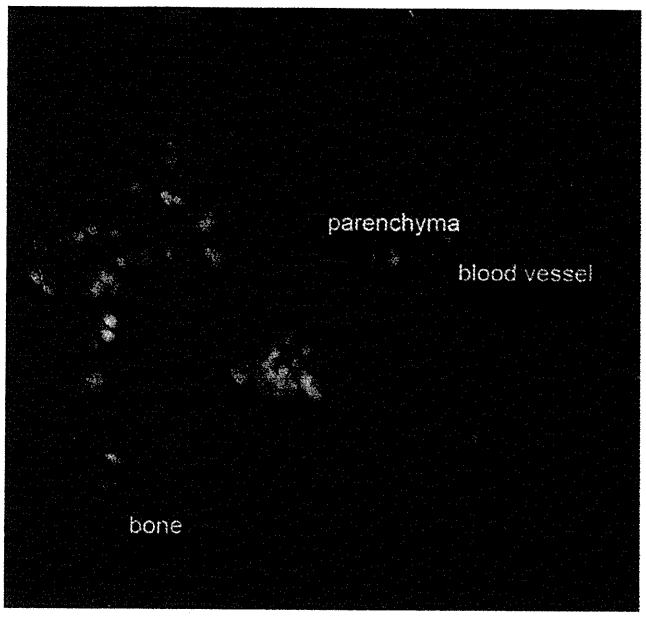

Figure 1 Stereoscopic view of bone marrow cavity visualised by intravital multiphoton imaging. Intravital imaging of the bone surface using multiphoton microscopy using CX_3CR1 promoter-driven EGFP-expressing mice. Blood vessels (red) and bone tissues (blue) were visualised by Texas Red-conjugated high-molecular dextrans (70 kDa) and second harmonic generation, respectively. Scale bars represent 30 μm.

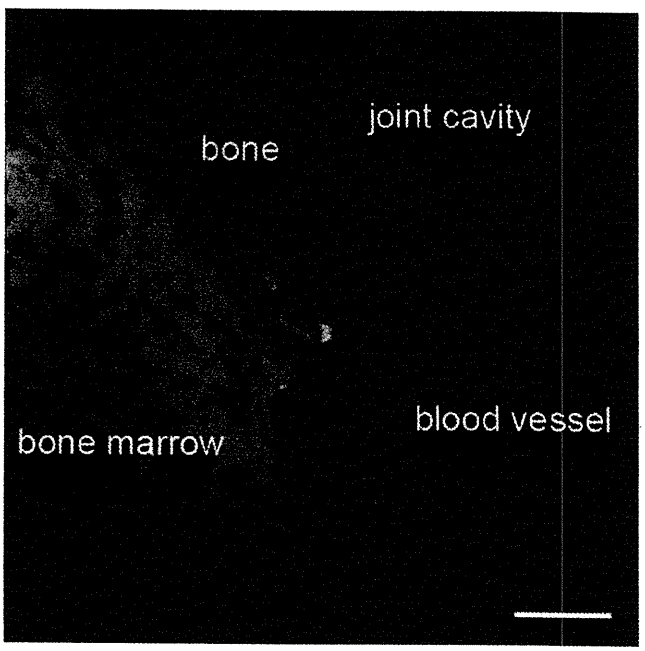

Figure 2 Intravital multiphoton imaging of a murine finger joint. Intravital imaging of a murine finger joint using multiphoton microscopy using LysM promoter-driven EGFP-expressing mice. Blood vessels (red) and bone tissues (blue) were visualised by Texas Red-conjugated high-molecular dextrans (70 kDa) and second harmonic generation, respectively. Scale bars represent 50 μm.

and lipid mediators, such as sphingosine-1-phosphate and CXC chemokine ligand 12.[13–15] Recently, we also successfully visualised the bone-resorbing activity of mature osteoclasts lining bone surfaces and identified their real mode of action in situ (manuscript submitted). Despite its hardness, the bone is a dynamic and elastic tissue that undergoes continuous remodelling by bone-resorbing osteoclasts and bone-replenishing osteoblasts. Inflammation and hormonal perturbation lead to the aberrant activation of osteoclasts, resulting in several bone-resorptive disorders, chiefly osteoporosis and rheumatoid arthritis (RA). Thus, osteoclasts have emerged as a good therapeutic target against these diseases, and the intravital imaging of bone tissues would be a good tool for the identification of novel target molecules and the development and evaluation of novel therapeutics.

USABILITY OF INTRAVITAL FLUORESCENT IMAGING TO REVEAL RA PATHOGENESIS

Intravital imaging is considered to be difficult because joints are surrounded by hard bone tissues and their structure is anatomically complex. To date, in vivo whole-body imaging with near-infrared optics has been used to detect inflammation in murine arthritic models,[16 17] although this modality is not capable of tracking cellular and molecular dynamics in arthritic joints in situ. Recently, we and other groups have sought to establish methods for the intravital multiphoton imaging of joints in physiological and pathological conditions, and we have recently succeeded in visualising the dynamic behaviour of inflammatory cells in live murine joints (figure 2).

The most remarkable advantage of intravital fluorescent microscopy is its high spatiotemporal resolution with the observation of differently coloured respective cells. By using this intravital fluorescent joint imaging system, we could detect complex cellular interactions in arthritic joints in situ in the future, which could lead to the discovery of autoimmune inflammation exacerbation, bone-erosive mechanisms and pathogenic events in a murine arthritis model. For example, by using time-lapse fluorescent imaging, we will be able to analyse the very initial events regarding the onset of arthritis, such as immune/stromal intercellular crosstalk and inflammatory cell activation, which

Ishii M. *Ann Rheum Dis* (2011). doi:10.1136/annrheumdis-2011-200599

would be critically useful for understanding pathogenic mechanisms of arthritis.

Different molecular-targeted biologics against RA could be tested using this new assay system to identify the critical point of control for therapeutics. Intravital imaging can also examine the time course of arthritis onset, which may be useful for identifying the pathogenic event of RA. Although the methodology has not yet been fully established, intravital fluorescent imaging of arthritic joints in the near future is sure to bring us a wealth of knowledge in the field of basic and clinical rheumatology. Due to the limited penetrance of visible light signals, it is hard to use fluorescent microscopy directly for elucidating human immunology (table 1). Nevertheless, recent developments on fluorescent endoscopy have enabled us to visualise local events in gastrointestinal tracts,[18] and such approach would be applicable also for arthroendoscopy in the future.

CLINICAL APPLICATION: NUCLEAR IMAGING FOR RA

Radioimaging modalities such as positron emission tomography (PET) could be beneficial for the evaluation of arthritis in humans. The system detects pairs of γ-rays emitted indirectly by a positron-emitting radionuclide tracer, which is introduced into the body on a biologically active molecule. Although the spatiotemporal resolution of PET is limited, the high signal-to-noise ratio enables us to detect phenomena deep inside the human body (table 1). Several previous PET studies have demonstrated localised joint inflammation in patients with RA with the use of ^{18}F-labelled fluorodeoxyglucose, an analogue of glucose analogue which is one of the most commonly used radioimaging probes for the detection of high-metabolising areas, such as inflammation and cancer.[19 20] The combined use of PET with other imaging modalities, such as MRI and CT, enables the visualisation of local synovial inflammation in RA. Recently, the dynamic behaviour of CD20$^+$ B cells in patients with RA has been detected using ^{124}I-labelled rituximab, a therapeutic anti-CD20 monoclonal antibody.[21] This kind of 'molecule-' or 'cell-targeted' radioimaging could become especially useful for analysing the pathophysiology of inflammation and bone erosion in RA.

The development and clinical application of biological agents have undoubtedly caused a paradigm shift in the therapeutics of RA, and several targets have been identified to date, such as tumour necrosis factor, interleukin (IL)-6 receptor, cytotoxic T lymphocyte antigen 4, IL-17 and Janus kinase 3. Several drugs have also been developed against tumour necrosis factor (eg, infliximab, etanercept, adalimumab, golimumab), and the next major consideration is the rational selection of appropriate therapeutics among these various drugs. Radiolabelled biological agents could be used to evaluate the involvement of the target molecule of interest in patients with RA and, thus, provide the clinician with information for making rational decisions in the selection of therapeutic agents. In addition, monitoring the status of targeted cytokines in patients may enable us to decide on the end point of the regimen. These developments will facilitate the creation of patient-specific regimens for patients with RA with the use of a wide array of therapeutic tools.

CONCLUSION

Major progress has been made recently in imaging techniques, and several tools for the visualisation of live biological systems in situ have become available. These tools must bring a paradigm shift in the field of basic and clinical rheumatology and lead to changes in the treatment of RA in the future.

Competing interests None.

Provenance and peer review Commissioned; externally peer reviewed.

REFERENCES

1. **Denk W**, Strickler JH, Webb WW. Two-photon laser scanning fluorescence microscopy. *Science* 1990;**248**:73–6.
2. **Cahalan MD**, Parker I, Wei SH, *et al.* Two-photon tissue imaging: seeing the immune system in a fresh light. *Nat Rev Immunol* 2002;**2**:872–80.
3. **Germain RN**, Miller MJ, Dustin ML, *et al.* Dynamic imaging of the immune system: progress, pitfalls and promise. *Nat Rev Immunol* 2006;**6**:497–507.
4. **Miller MJ**, Wei SH, Parker I, *et al.* Two-photon imaging of lymphocyte motility and antigen response in intact lymph node. *Science* 2002;**296**:1869–73.
5. **Garside P**, Brewer JM. Real-time imaging of the cellular interactions underlying tolerance, priming, and responses to infection. *Immunol Rev* 2008;**221**:130–46.
6. **Germain RN**, Bajénoff M, Castellino F, *et al.* Making friends in out-of-the-way places: how cells of the immune system get together and how they conduct their business as revealed by intravital imaging. *Immunol Rev* 2008;**221**:163–81.
7. **Bousso P**, Bhakta NR, Lewis RS, *et al.* Dynamics of thymocyte-stromal cell interactions visualized by two-photon microscopy. *Science* 2002;**296**:1876–80.
8. **Deane JA**, Hickey MJ. Molecular mechanisms of leukocyte trafficking in T-cell-mediated skin inflammation: insights from intravital imaging. *Expert Rev Mol Med* 2009;**11**:e25.
9. **Kreisel D**, Nava RG, Li W, *et al. In vivo* two-photon imaging reveals monocyte-dependent neutrophil extravasation during pulmonary inflammation. *Proc Natl Acad Sci USA* 2010;**107**:18073–8.
10. **Egen JG**, Rothfuchs AG, Feng CG, *et al.* Macrophage and T cell dynamics during the development and disintegration of mycobacterial granulomas. *Immunity* 2008;**28**:271–84.
11. **Chieppa M**, Rescigno M, Huang AY, *et al.* Dynamic imaging of dendritic cell extension into the small bowel lumen in response to epithelial cell TLR engagement. *J Exp Med* 2006;**203**:2841–52.
12. **Mazo IB**, Honczarenko M, Leung H, *et al.* Bone marrow is a major reservoir and site of recruitment for central memory CD8+ T cells. *Immunity* 2005;**22**:259–70.
13. **Ishii M**, Egen JG, Klauschen F, *et al.* Sphingosine-1-phosphate mobilizes osteoclast precursors and regulates bone homeostasis. *Nature* 2009;**458**:524–8.
14. **Klauschen F**, Ishii M, Qi H, *et al.* Quantifying cellular interaction dynamics in 3D fluorescence microscopy data. *Nat Protoc* 2009;**4**:1305–11.
15. **Ishii M**, Kikuta J, Shimazu Y, *et al.* Chemorepulsion by blood S1P regulates osteoclast precursor mobilization and bone remodeling in vivo. *J Exp Med* 2010;**207**:2793–8.
16. **Chen WT**, Mahmood U, Weissleder R, *et al.* Arthritis imaging using a near-infrared fluorescence folate-targeted probe. *Arthritis Res Ther* 2005;**7**:R310–7.
17. **Gompels LL**, Madden L, Lim NH, *et al. In vivo* fluorescence imaging of E-selectin: quantitative detection of endothelial activation in a mouse model of arthritis. *Arthritis Rheum* 2011;**63**:107–17.
18. **Urano Y**, Asanuma D, Hama Y, *et al.* Selective molecular imaging of viable cancer cells with pH-activatable fluorescence probes. *Nat Med* 2009;**15**:104–9.
19. **Kubota K**, Ito K, Morooka M, *et al.* FDG PET for rheumatoid arthritis: basic considerations and whole-body PET/CT. *Ann N Y Acad Sci* 2011;**1228**:29–38.
20. **Miese F**, Scherer A, Ostendorf B, *et al.* Hybrid (18)F-FDG PET-MRI of the hand in rheumatoid arthritis: initial results. *Clin Rheumatol* 2011;**30**:1247–50.
21. **Tran L**, Huitema AD, van Rijswijk MH, *et al.* CD20 antigen imaging with ^{124}I-rituximab PET/CT in patients with rheumatoid arthritis. *Hum Antibodies* 2011;**20**:29–35.

Chapter 10

Use of Intravital Microscopy and In Vitro Chemotaxis Assays to Study the Roles of Sphingosine-1-Phosphate in Bone Homeostasis

Taeko Ishii, Shunsuke Kawamura, Issei Nishiyama, Junichi Kikuta, and Masaru Ishii

Abstract

We describe a method to visualize the migration of osteoclast precursors within intact murine bone marrow in real time using intravital multiphoton microscopy. Conventionally, cell migration has been evaluated using in vitro systems, such as transmigration assays. Although these methods are convenient for quantification and are highly reproducible, these in vitro assay systems may not accurately reflect in vivo cellular behavior. In addition to in vitro analyses, recent technological progress in two-photon excitation-based laser microscopy has enabled the visualization of dynamic cell behavior deep inside intact living organs. Combining this imaging method with in vitro chemoattraction analyses, we have revealed that sphingosine-1-phosphate (S1P), a lipid mediator enriched in blood, bidirectionally controls the trafficking of osteoclast precursors between the circulation and bone marrow cavities via G protein-coupled receptors (GPCRs).

Key words: Intravital imaging, Multiphoton microscopy, Migration, Osteoclast precursor, S1P, S1PR1, S1PR2

1. Introduction

Bone is a dynamically regulated organ that continuously undergoes remodeling to maintain mineral homeostasis and structural robustness during growth and even in adulthood (1, 2). The balance between bone resorption by osteoclasts and bone formation by osteoblasts is finely regulated. During differentiation, osteoclasts and osteoblasts interact with and regulate each other (3). Recently, recruitment of osteoclast precursors was identified to

Alice Pébay and Kursad Turksen (eds.), *Sphingosine-1-Phosphate: Methods and Protocols*, Methods in Molecular Biology, vol. 874,
DOI 10.1007/978-1-61779-800-9_10, © Springer Science+Business Media, LLC 2012

be a critical control mechanism that maintains bone homeostasis (4–13). Osteoclasts are bone-resorbing, multinucleated giant cells that stem from mononuclear macrophage/monocyte-lineage hematopoietic precursors (2). These precursors are recruited at the correct time to appropriate sites for differentiation. We have developed a novel intravital multiphoton imaging system for visualizing the highly organized migration of osteoclast precursors between the bone marrow and blood vessels with high spatiotemporal resolution (13, 14). This new intravital imaging method showed that the bioactive lipid sphingosine-1-phosphate (S1P) controls the migratory behavior of osteoclast precursors in concert with various chemokines.

Multiphoton (usually two-photon) excitation-based laser microscopy has enabled visualization of living cells in intact living organs and analysis of their mobility and interactions quantitatively (15–18). The penetration depths of two-photon microscopy depend on the composition of the tissues. In contrast to soft tissues, such as the brain cortex, in which the penetration depth is 800–1,000 μm, accessing deep inside bone tissues is difficult. However, in the mouse parietal bone, the distance from the bone surface to the bone marrow cavity is only ~80–120 μm and within the range of two-photon microscopy. At this region, we can access the living bone marrow with minimal invasion. To observe cells with two-photon microscopy, they must be fluorescently labeled. We have used transgenic mice in which enhanced green fluorescent protein (EGFP) is expressed under the control of the promoter of CX_3CR1 (a CX_3CL1/fractalkine receptor) (19) or CSF1R (20), which are activated in monocytoid cells, including osteoclast precursors. Subsequently, we set up the platform to visualize the behavior of osteoclast precursors in a living body.

S1P transmits its signal through five 7-transmembrane receptors or G-protein-coupled receptors (GPCRs), named S1PR1 to S1PR5 (21). Among them, osteoclast precursors express S1PR1 and S1PR2 (13). S1PR1 activates Rac through G_i and promotes cell migration and intercellular connections, while S1PR2 conjugates $G_{12/13}$ and activates Rho pathways, which counteract S1PR1, thus inhibiting Rac activity (21). To clarify S1P function through each receptor, we intravenously injected FTY720 (22), an agonist for four of the five S1P receptors (all except S1PR2), a potent S1PR1 specific agonist SEW2871 (23), or a potent S1PR2 antagonist JTE013 (24) and then observed the mobility of osteoclast precursors.

In addition to this new imaging technique, to clarify the bidirectional chemotactic function of S1P concerning osteoclast precursors, we performed in vitro chemotaxis analysis with high and low concentrations of S1P using EZ-TAXIScan (14). This device enables visualization of the mobility of cells in real time in vitro.

In a high S1P environment, such as the blood circulation, S1PR1 is first activated and rapidly internalized, while S1PR2 is predominant. Osteoclast precursors enter bone marrow by chemorepulsion through S1PR2 and other chemokines attract them to the bone surface. In a low S1P environment, such as the bone marrow, as S1PR1 is restored on the cell surface, osteoclast precursors can recirculate from bone tissues to blood vessels through chemotaxis by the S1P gradient.

2. Materials

2.1. Multiphoton Microscopy

1. Upright microscope (DM6000B; Leica Microsystems) equipped with a 20× water immersion objective (HCX APO: numerical aperture (NA), 1.0; working distance)WD), 2.0 mm; Leica Microsystems) (see Note 1).
2. Femtosecond-pulsed infrared laser (MaiTai HP Ti:Sapphire laser; Spectra-Physics; see Note 2).
3. A non-descanned detector (NDD) that has 2–4 channels (see Note 3).
4. Customized microscope stage (see Note 4).
5. An environmental chamber in which anesthetized mice are warmed at 37°C by an air heater (see Note 5).

2.2. Anesthesia

1. Male or female CX_3CR1-EGFP knock-in mice (19), CSF1R(M-CSF receptor)-EGFP transgenic mice (20), osteoclast/monocyte-specific S1PR1-deficient mice, generated by crossing mice bearing conditional S1PR1 knockout alleles ($S1PR1^{loxP}$) (25) to transgenic mice expressing Cre under the Cd11b promoter (26) (see Note 6), and S1PR2-deficient mice (ref. 27; see Note 7).
2. Knockout mice are used with their wild-type (WT) littermates as the control.
3. Isoflurane (Escain).
4. Inhalation anesthesia apparatus (Baxter; 2.5% vaporized in an 80:20 mixture of O_2 and air).
5. Anesthesia box and mask.

2.3. Preparation of Mice

1. Custom-made stereotactic holder that can immobilize a mouse's head with fixing at three points—both ears and the foreteeth (Fig. 1).
2. Shaver and hair-removal lotion (Epilat).
3. Iris scissors and tweezers for mouse operation.
4. O-ring: a 1.5-mL microtube is cut into a 2-mm thick slice (see Note 8).

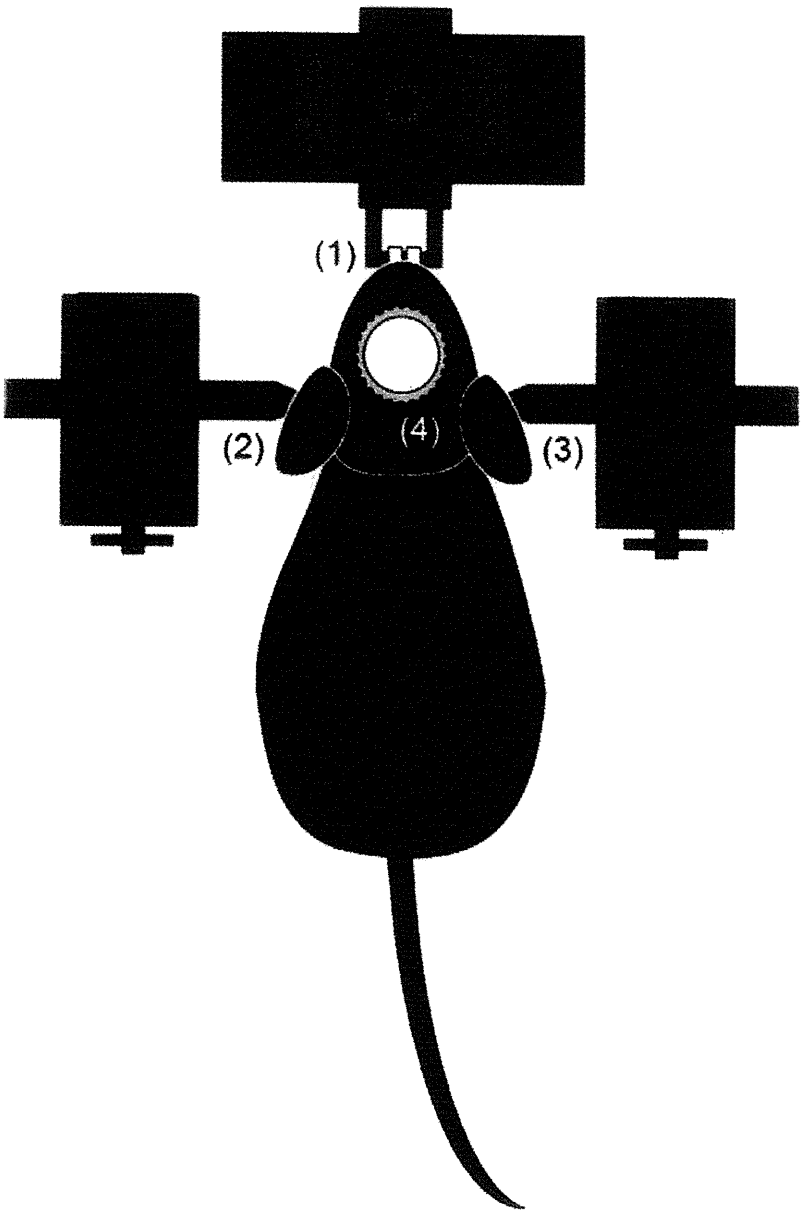

[AU1]

Fig. 1. Schematic illustration of how to fix a mouse on the stage. The mouse's head is immobilized with fixing at three points: foreteeth (1) and both ears (2 and 3). The O-ring is inserted into the incision of the skin and is filled with PBS (4).

5. Instant adhesive and petrolatum or Difloil grease.
6. Phosphate-buffered saline (PBS) immersion buffer, pH 7.4.

2.4. Staining of Blood Vessels

1. Angiographic agent: 2 mg/mL of 70-kDa Texas Red-conjugated dextran in PBS (see Note 9).
2. 29 or 30-G insulin syringes (Becton Dickinson) for intravenous injection.

2.5. Treatment with Reagents

1. FTY720 (3 mg/kg; Cayman Chemical) dissolved in a vehicle [PBS containing 5% acidified dimethylsulfoxide (DMSO) and 3% fatty acid-free bovine serum albumin (BSA)] or vehicle (22).